

# Learning Physically Realizable Skills for Online Packing of General 3D Shapes

ANONYMOUS AUTHOR(S)

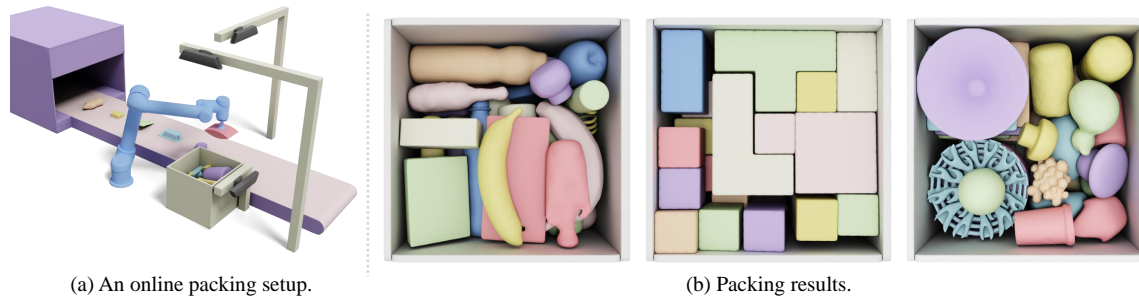


Fig. 1. We develop a learning-based solver for packing arbitrary-shaped objects in a physically realizable problem setting. This figure shows an online virtual packing setup (a), where objects move on a conveyor belt at a constant speed. Three RGB-D cameras are provided for observing the top and bottom surfaces of the incoming object as well as packed object configurations inside the container. Within a limited time window, the robot has to decide on the placement for the incoming object in the target container for tight packing. Packing results on 3D shapes with different geometric properties are shown in (b).

We study the problem of learning *online* packing skills for *irregular 3D shapes*, which is arguably the most challenging setting of bin packing problems. The goal is to consecutively move a sequence of 3D objects with arbitrary shapes into a designated container with only partial observations of the object sequence. Meanwhile, we take physical realizability into account, involving physics dynamics and constraints of a placement. The packing policy should understand the 3D geometry of the object to be packed and make effective decisions to accommodate it in the container in a physically realizable way. We propose a Reinforcement Learning (RL) pipeline to learn the policy. The complex irregular geometry and imperfect object placement together lead to huge solution space. Direct training in such space is prohibitively data intensive. We instead propose a theoretically-provable method for candidate action generation to reduce the action space of RL and the learning burden. A parameterized policy is then learned to select the best placement from the candidates. Equipped with an efficient method of asynchronous RL acceleration and a data preparation process of simulation-ready training sequences, a mature packing policy can be trained in a physics-based environment within 48 hours. Through extensive evaluation on a variety of real-life shape datasets and comparisons with state-of-the-art baselines, we demonstrate that our method outperforms the best-performing baseline on all datasets by at least 12.8% in terms of packing utility.

CCS Concepts: • **Computing methodologies** → **Shape analysis**.

Additional Key Words and Phrases: irregular shapes, 3D packing problem, reinforcement learning, combinatorial optimization

## 1 INTRODUCTION

The problem of packing, i.e., finding an efficient placement of as many as possible objects within a designated volume, has garnered a multidisciplinary research interest from combinatorial optimization [Martello et al. 2000; Seiden 2002], computational geometry [Hu et al. 2020; Ma et al. 2018] and machine learning [Hu et al. 2017; Zhao et al. 2022a].

More than four centuries ago, the famous Kepler conjecture already considered the continuous packing of spheres in infinite spaces, which has been proved only recently [Hales et al. 2017]. Even the discrete bin packing problem has been proven NP-hard [Hartmanis 1982]. For 3D shape packing, most existing works consider simple object shapes such as cuboids [Martello et al. 2000], tetrahedra [Conway and Torquato 2006], or ellipsoids [Kallrath 2017]. The more general problem of *irregular shape packing*, on the other hand, has received much less study, although being practically useful in many real application scenarios. In robotics, product packing robots [Shome et al. 2019; Wang and Hauser 2019, 2021; Yang et al. 2021] for logistics automation is an active research area. In computer graphics, irregular shape packing has been widely explored in UV atlas generation [Limper et al. 2018; Liu et al. 2019; Zhang et al. 2020], artistic puzzle design [Chen et al. 2022; Wang et al. 2021], 2D panel fabrication [Saakes et al. 2013], and 3D printing [Chen et al. 2015], with various constraints.

We study the problem of irregular shape packing through the lens of practically feasible robotic packing, namely *Physically Realizable Packing (PRP)*. In particular, PRP combines two well-known robotic tasks, pick-and-place [Han et al. 2019] and irregular shape packing [Wang and Hauser 2019], while further requiring packed objects governed by physics dynamics. As illustrated in Fig. 1, our virtual problem setup involves a robot arm equipped with a sucker-type gripper. Irregularly shaped objects are transported by a conveyor belt in a planar-stable pose and move at a constant speed. The upper surface of the object is captured by a top-view camera and the robot can move this object above an up-looking camera to capture its bottom surface. We pursue an online setting [Seiden 2002] where the robot observes only the object coming in the next instead of the full sequence. After the robot releases each object at its planned configuration inside the target container, we use a full-fledged physics simulator [Coumans and Bai 2016], compatible with the standard RL learning platform [Brockman et al. 2016], to determine the ultimate quasi-static pose of all objects and enforce physically realizable constraints. Our physics constraint accounts for both quasi-static and dynamic interactions between objects, generalizing the prior pile stability constraint [Wang and Hauser 2019] which only considers quasi-static interactions.

We propose a novel Reinforcement Learning (RL) pipeline to train effective packing policies. The sequential nature of packing has stimulated several recent RL-based approaches [Hu et al. 2020; Zhao et al. 2021, 2022a]. Compared with manually designed heuristics [Ha et al. 2017; Karabulut and Inceoglu 2004; Ramos et al. 2016], RL is capable of learning complex application-side constraints from guided explorations. RL also bears the potential to outperform humans on both continuous and discrete decision-making problems [Duan et al. 2016; Mnih et al. 2015]. However, prior RL-based approaches opt to factor out the continuous aspect of the problem and only learn a discrete packing policy, via assuming cuboid objects and omitting physics constraints. The continuous nature of the irregular shape packing problem calls for exploiting the full potential of RL through accounting for physics constraints. We contribute a practical algorithm to learn packing policies for irregular 3D shapes via overcoming a series of technical challenges.

First of all, learning effective packing policies is naturally a tough challenge. The complex irregular geometry and imperfect object placement due to physics dynamics together lead to huge solution space. Direct policy training through trial and error in such spaces is prohibitively data intensive. We instead propose a candidate action generation method to reduce the action space of RL as well as the learning burden. The candidates are the convex vertices of the (polygonal) connected regions within which the current object can be placed. We prove that these candidates are local optima that make the object tightly packed against the obstacles (the placed objects and the container). Our learned policy is then used to understand the geometry of the current object and choose the best placement from its corresponding candidates. This method significantly reduces the search space of RL and enables reliable learning of packing policies.

Both the geometry understanding and the candidate selection need a gazillion experiences collected through simulation. However, interaction with the simulation world is CPU-bound and is time-consuming, which leaves policies less trained per wall-clock time. Some abnormally slow instances also block the uniform training schedule. To this end, we propose to accelerate the training via an asynchronous sampling strategy. In particular, we decouple the training into a parallelized experience sampling process for non-blocking treatment and a separate learning process for continuously updating parameters. Our method allows a robust packing policy to be trained within 48 hours on a desktop machine.

In addition, RL algorithms should be trained with sufficient data variety to ensure the robustness of the learned policies. As compared with cubical shape packing, however, the variety of object shapes and poses for irregular shape packing is on a much higher level. We propose a data preparation process for generating sequences of simulation-ready objects each with a planar-stable pose. Working with a combination of several real-world and synthetic datasets, we create a packing problem generator emitting randomized, versatile, and faithful problem instances.

We have conducted extensive evaluations of our method on well-established datasets with various geometric characteristics. By comparing with a row of baseline algorithms, we demonstrate that our method significantly outperforms the best-performing baseline on all datasets by at least 12.8% in terms of packing utility. Furthermore, we extend our method to the scenario of buffered packing, where the robot maintains a buffer for re-ordering objects, and show that higher packing quality can be achieved. Our contributions include:

- An effective and theoretically-provable placement candidate generation method for pruning the action space of RL, along with a learnable pack policy for candidate selection.
- An efficient, asynchronous, off-policy sampling strategy for accelerating packing policy training.
- A constructive PRP environment modeling realistic packing with a large object dataset and RL-compatible interfaces.

## 2 RELATED WORK

Our work is built off of prior works on packing policy searches. Our problem is also closely related to other packing-related tasks in computer graphics and robotics.

### 2.1 Packing Policies

Being an NP-hard problem, various heuristic policies have been proposed for 2D [Lodi et al. 2002] and 3D [Ali et al. 2022] cubical object packing over time, without a single best performer. The transition of focus to irregular shapes is quite recent. Liu et al. [2015] pack irregular 3D shapes using a Minimum-Total-Potential-Energy (MTPE) heuristic and prioritize shapes with the lowest gravitational center of height. Wang and Hauser [2019] propose the Heightmap Minimization (HM) heuristic to minimize the volume increase of packed non-convex shapes as observed from the loading direction. Goyal and Deng [2020] make their packing decision via the Bottom-Left-Back-Fill (BLBF) heuristic [Tiwari et al. 2010], which places an object in the bottom-most, left-most, and back-most corner. All these placement rules are manually designed based on specific observations, which limits their applicability. For example, the HM heuristic performs quite well for non-convex shape packing, since it aims to minimize space occupancy vertically. However, it cannot differentiate horizontal placements on a flat container, leading to sub-optimal cases demonstrated in Fig. 2a.

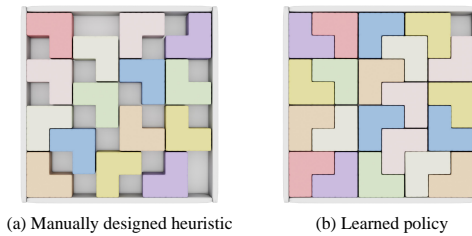


Fig. 2. When packing simple polyominoes in a flat container, the result generated using the HM heuristic (a) exhibits a non-trivial sub-optimality gap as compared with that of our learned policy (b).

The latest efforts [Duan et al. 2019; Hu et al. 2017, 2020; Zhao et al. 2021, 2022a] resort to machine learning, specifically RL, to automatically synthesize policies that work well on an arbitrary cubical shape packing task without human intervention. Early works [Duan et al. 2019; Hu et al. 2017, 2020], however, only learn the order of cuboids to be packed, while using separate heuristics or algorithms to compute the placement. More recent work [Zhao et al. 2021] learns the placement policy via predicting logits of discretized placement locations. The latest work [Zhao et al. 2022a] combines the merit of heuristic and learning-based policies using a candidate selection policy parameterization, having the policy rank a pre-defined set of candidate placements. Our policy inherits these ideas with necessary modifications toward irregular shapes.

## 2.2 Packing in Computer Graphics

There is a handful of packing-related graphic problems, most of which involve irregular shapes and continuous decision variables. UV atlas generation, for example, minimizes the memory footprint by packing many texture charts into a single texture image. To generate high-quality textures, an algorithm needs to jointly optimize irregular chart shapes and their continuous packing placements. Early works [Lévy et al. 2002; Ray et al. 2003] nail down the two classes of decision variables in separate sub-stages. More recent works [Limper et al. 2018; Liu et al. 2019; Zhang et al. 2020] couple the two sub-stages by decomposing the charts for higher packing efficacy. Limper et al. [2018] propose a heuristic strategy to iteratively cut charts into smaller ones and repack them using heuristics [Nöll and Strieker 2011]. However, the shape of chart boundaries is pre-determined and cannot be modified during cutting. Liu et al. [2019] and Zhang et al. [2020] propose to deform charts into rectangular patches and then adopt rectangular packing heuristics [Schertler et al. 2018]. But their work is irrespective of the sequential nature of the packing problem, deforming chart shapes in a sub-stage.

A similar requirement to UV atlas generation arises in 3D printing, where the limited volume of commodity 3D printers requires large objects to be partitioned and/or repacked for printing efficacy. The packing plan can be further constrained for manufacturability and structure robustness. The first work [Luo et al. 2012] in this direction cuts large objects using the BSP-tree, such that each leaf node fits into the printing volume. They choose cutting planes from the object surface patches, essentially discretizing the continuous solutions. Luo et al. [2012] select BSP-tree structures guided by a score function incorporating various constraints. However, their optimization strategy is myopic, i.e., using a horizon equal to one. Their follow-up work [Yao et al. 2015] further allows irregular part shapes to be locally optimized for structure robustness and collision resolution, and then packs the parts into the printing volume using local numerical optimization. As a result, Yao et al. [2015] allow continuous optimization of both irregular object shapes and packing

placements, but their optimizer is still myopic. A similar approach has been proposed by Ma et al. [2018], which only optimizes the final object placement result and neglects the packing process.

Our problem is closely related to these works by optimizing online placements for general 3D shapes. Modeling packing as a sequential-decision making problem, our method bears the potential of closing the sub-optimality gap as illustrated in Fig. 2b. A related work to ours is TAP-Net [Hu et al. 2020], which considers sequential object selection and packing problem in a discrete state-action space, assuming cubical objects and perfect placement without physics dynamics. Our method deviates from [Hu et al. 2020] in two important ways. First, we assume continuous object placements and physics realizability constraints. This is a much more realistic setting mimicking real-world packing problems. Our physics simulator allows uncertainty to be modeled, lifting the assumption of perfect policy execution. Second, our policy parameterization enables the RL algorithm to directly train the entire policy end-to-end, instead of only the object selection policy as done in [Hu et al. 2020], which is one reason for our superior performance over all existing baselines.

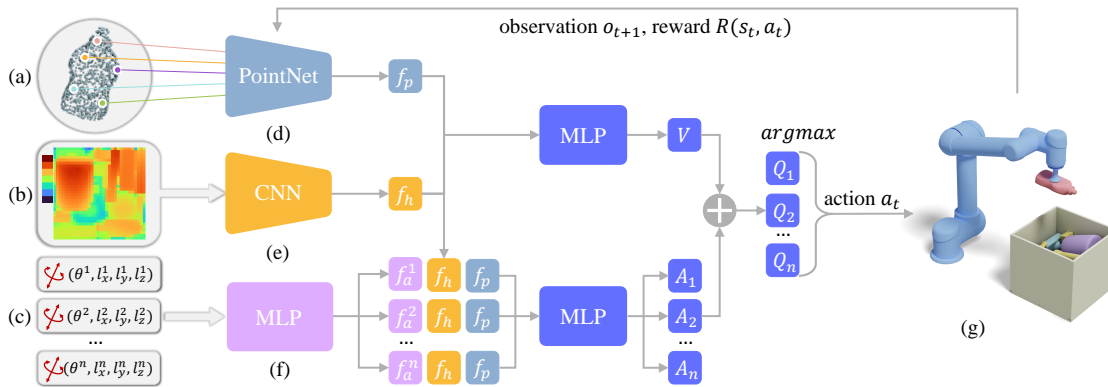


Fig. 3. Our policy learning architecture. The input to our method is the surface point cloud (a) of the incoming object,  $P$ , and the heightmap (b) of continuous object configurations in the target container,  $H_c$ . Our neural network policy uses PointNet (d) and CNN (e) to extract features of  $P$  and  $H_c$  respectively for 3D geometry understanding. Our geometric-inspired candidate generalization method would then provide a set of placements (c), each encoded as a feature  $f_a^i$  using an MLP (f). Finally, our policy which is a dueling network ranks the placement candidates via the state-action value function  $Q$ , and the best candidate is selected for execution. The continuous object configurations inside the target container are governed by a physics simulator (g). The packing process continues with receiving the next observation until the container is full. Our RL algorithm trains the ranking policy by asynchronously sampling trajectories and updating policy parameters with granted reward signals.

### 2.3 Packing in Robotics

Roboticians consider packing as a component in the pipeline of perception, planning, predicting, and control, rather than a standalone algorithmic problem. However, the progress in robotic packing tasks is relatively slow. This is because the robust execution of high-quality packing plans is extremely difficult due to the tiny spaces between objects. We are only aware of two prior works [Shome et al. 2019; Wang and Hauser 2019] presenting full-featured packing systems. Wang and Hauser [2019] use a robot arm with a sucker-type gripper to grab objects from top-down views. Their following work [Wang and Hauser 2022] further introduces a fallback strategy to shake the target container and create new open spaces for packing. Shome et al. [2019] restart the sensing, motion planning, and control loop whenever failures are

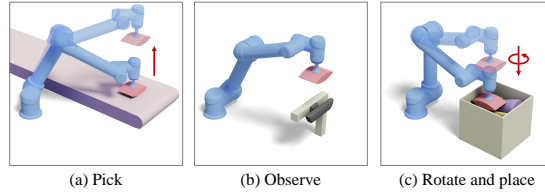


Fig. 4. Snapshots of robot manipulations. The robot picks up the incoming object (a) from the conveyor belt and moves this object above an up-looking camera to observe the bottom surface (b). Then, the robot adjusts the vertical orientation of the object and places it in the container (c). The robot only picks and places an object from a top-down view.

detected in the downstream stages. Both methods use simple heuristics to solve the underlying packing problem, with Wang and Hauser [2019] relying on the heightmap minimization heuristic and Shome et al. [2019] assuming known cubical object shapes and compatible target container sizes.

In contrast, bin-picking [Mahler and Goldberg 2017; Mahler et al. 2016] can be robustly executed on robot hardware, because the target container is assumed to be much larger than objects, rendering packing unimportant. The bin-picking solutions [Mahler and Goldberg 2017; Mahler et al. 2016], though quite different from ours, share commonality with our policy design. Both methods assume the availability of a set of candidate actions, which is then ranked by a learning-based policy. Most recently, Zeng et al. [2020] and Huang et al. [2022] bring the accuracy and generality of learning-based object transfer policy to another level by introducing equivalency. By factoring out the 2D rigid rotations from the neural network input-output space, learning becomes much more sample-efficient. We adopt a similar approach for factoring out rigid rotations during the forward calculation of packing policies.

### 3 METHOD

We introduce our online packing problem setup in Section 3.1 and formulate it as Markov Decision Process (MDP) in Section 3.2. To effectively solve this problem, we design a novel packing pattern based on candidate actions generated by a theoretically-provable method in Section 3.3. In Section 3.4, we describe our asynchronous RL algorithm for accelerating packing policy training in the physics simulation world. Extensions to buffered packing scenarios will be discussed in Section 3.5. The pipeline of our learning-based algorithm is outlined in Fig. 3.

#### 3.1 Problem Statement

Irregular shape packing problem considers a finite set of  $N$  geometric objects  $G_1, \dots, G_N$ . Each  $G_i \subset \mathbb{R}^3$  (in its local frame of reference) is of an irregular and possibly non-convex shape. Following the conventional Bin Packing Problem [Martello et al. 2000] (BPP), the target container  $C \subset \mathbb{R}^3$  takes up the space  $[0, S_x] \times [0, S_y] \times [0, S_z] \subset \mathbb{R}^3$ . The goal is to move as many objects into  $C$  in a collision-free and physically realizable manner and maximize the packing utility:

$$\sum_{G_i \subset C} |G_i|/|C|, \quad (1)$$

where  $|G_i|$  and  $|C|$  are the volume of object  $G_i$  and the container volume, respectively.

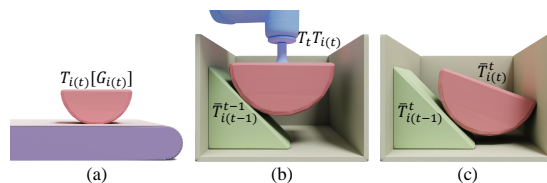


Fig. 5. (a): The object  $G_{i(t)}$  is transported by the conveyor with its planar-stable pose  $T_{i(t)}[G_{i(t)}]$ , at time step  $t$ . (b): The robot moves this object into the container and releases it with transform  $T_t T_{i(t)}$ . (c): Governed by rigid body dynamics, the ultimate continuous configuration for  $G_{i(t)}$  is  $\bar{T}_{i(t)}^t$ .

**3.1.1 Environmental Setup.** To mimic the real-world scenario of pick-and-place tasks, we assume that objects are stably laid on the conveyor belt moving at a constant speed, leaving the robot with a limited time window to pick up and place each  $G_i$  into  $C$ . Clearly, the time window size is a complex function of conveyor belt speed, robot motion speed, and various system delays. However, these factors can be tuned for different hardware platforms and are out of the scope of this work. We assume a fixed time window size, which allows us to model object packing as a sequential-decision problem. We postulate that the robot arm is equipped with a sucker-type gripper that can only pick and place an object from the top, as illustrated in Fig. 4, and that any object and any placement location in  $C$  can be reached by the robot. The robot can also apply a 1D rotation of the gripper around the Z-axis (vertical), the same assumption is adopted in [Zhao et al. 2022a]. Therefore, the space for robot decision is  $\mathbb{R}^3 \times SO(1)$ , consisting of a 3D position and an in-plane rotation.

To make packing decisions, the robot is equipped with three RGB-D cameras to fully observe the packing environment, as demonstrated in Fig. 1a. The on-conveyor camera is used for capturing the top surface of the incoming object while the on-container camera observes the continuous packing configurations inside the container. After picking up the incoming object, the robot moves it over a third, up-looking camera to capture its bottom surface, as shown in Fig. 4b, thus fully observing the geometry of the object to be packed.

Different from those works which only optimize the final packing result [Ma et al. 2018], PRP also concerns the packing process, i.e., moving the objects into the container one by one. Since the robot can only observe one object at a time, our packing problem follows the *online* setting [Seiden 2002] where each object is placed without the knowledge of the next ones. No further adjustment, such as unloading or readjusting, will be allowed. The robot must make an immediate decision that accommodates the incoming object while optimizing the overall compactness of the in-container layout. Packing alone is already a difficult combinatorial optimization problem, the arbitrarily complex object geometry and the imperfect placement make this problem even more challenging with huge solution space. We resort to RL to learn this packing skill automatically.

**3.1.2 Stable Object Poses.** As compared with BPP problems which only consider 6 axis-aligned orientations of cuboids, an irregular 3D object can have an arbitrary local-to-world orientation spanning the entire  $SO(3)$ . However, we can adopt a mild assumption that objects are stably lying on the conveyor belt with force equilibrium. This assumption holds when the conveyor belt has sufficient frictional forces and moves reasonably slowly, which is generally the case. We denote the incoming object id at the  $t$ th timestep as  $i(t)$ . Mathematically,  $G_{i(t)}$  is subject to a world transform  $T_{i(t)}$  such that  $T_{i(t)}[G_{i(t)}] \subset \mathbb{R}^3$  is a physically stable pose on the conveyor belt as Fig. 5a. The robot can then apply a vertical rigid transformation  $T_t \triangleq T(\theta, l_x, l_y, l_z)$  such that  $(T_t T_{i(t)})[G_{i(t)}] \subset C$  and  $(T_t T_{i(t)})[G_{i(t)}]$  is collision-free

with the boundary of  $C$  or any other objects already in  $C$ , as shown in Fig. 5b. Here  $\theta$  is the vertical rotation angle and  $(l_x, l_y, l_z)$  the 3D target position which takes the Front-Left-Bottom (FLB) of the Axis-Aligned Bounding Box (AABB) of  $G_{i(t)}$  as the reference point. Finally, the robot releases  $G_{i(t)}$  with  $T_t T_{i(t)}$  and the ultimate continuous configurations of all placed objects  $G_{i(1)}, \dots, G_{i(t)}$ , denoted as  $\bar{T}_{i(1)}^t, \dots, \bar{T}_{i(t)}^t$ , are governed by rigid body physics dynamics like Fig. 5c.

### 3.2 PRP Learning Environment

In this section, we discuss our PRP environment compatible with all statements of Section 3.1. This involves a random packing problem emission procedure and an environment model that casts online packing as a Markov Decision Process for RL training.

*Problem Emission.* We aim at learning packing skills for 3D shapes of a specific data distribution, so the training and testing sequences are generated with objects from the same object dataset. The sequences are randomly generated and are not shared by training and testing. Although this is a typical assumption by most policy learning works, we will demonstrate the generalization of our method to out-of-distribution objects in Section 4.4. Given a shape set, we emit a random packing problem (a sequence of posed objects) by first picking a random shape from the dataset and then selecting a stable pose for it, both with uniform probability and bootstrap sampling. Then, the vertical in-plane orientation of an object is also uniformly randomized. The sampling is repeated until the objects of the sequence are enough to fill the container ( $\sum_i |G_i| > |C|$ ).

*Markov Decision Process.* Our online packing problem can be formulated as a Markov Decision Process, which is a tuple  $\langle \mathcal{S}, \mathcal{A}, \mathcal{P}, R, \gamma \rangle$ . During each step  $t$  of the decision, an agent observes the (partial) state  $s_t \in \mathcal{S}$  of the current environment and makes a decision  $a_t \in \mathcal{A}$ , where  $\mathcal{S}$  and  $\mathcal{A}$  are the state space and the action space, respectively. The environment then responds by bringing  $s_t$  to  $s_{t+1}$  via a stochastic transition function  $s_{t+1} \sim \mathcal{P}(s_t, a_t)$  and granting a reward  $R(s_t, a_t)$ . The agent is modeled as a policy function  $a_t \sim \pi(o(s_t), \omega)$ , where  $o$  is the observation function and  $\omega$  the parameter of  $\pi$ . Under this setting, solving the online packing problem amounts to the following stochastic optimization:

$$\operatorname{argmax}_{\omega} \mathbb{E}_{s_0 \sim I, \tau \sim \pi, \mathcal{P}} \left[ \sum_{t=0}^{\infty} \gamma^t R(s_t, a_t) \right], \quad (2)$$

where  $I$  is the stochastic problem emitter,  $\gamma$  is a constant discount factor, and  $\tau = (s_0, a_0, s_1, \dots)$  is a sampled trajectory. Below we postulate each component of our MDP, putting together to form our packing environment.

*State Space  $\mathcal{S}$  and Transition Function  $\mathcal{P}$ .* At timestep  $t$ , the true state of the current environment involves ultimate object configurations inside the target container and the state of the incoming object, i.e.:

$$s_t \triangleq \langle \bar{T}_{i(1)}^{t-1} [G_{i(1)}], \dots, \bar{T}_{i(t-1)}^{t-1} [G_{i(t-1)}], T_{i(t)} [G_{i(t)}] \rangle,$$

essentially mimicking the online packing setting. The robot applies a temporary, initial transform  $T(\theta, l_x, l_y, l_z) T_{i(t)}$  for the  $i(t)$ th object. After that, our transition function, aka., the rigid body simulator [Coumans and Bai 2016], then integrates the poses of all  $t$  objects to reach force equilibrium. We decide that all objects have reached force equilibrium



when they have a velocity magnitude smaller than some threshold. At the force equilibrium state, we check for any objects that fall outside  $C$  or have a height beyond  $C$ , in which case we terminate the episode.

*Observation Function  $o$ .* We provide enough RGB-D cameras for capturing continuous object configurations inside container  $C$  and the top/bottom surface of the incoming object  $T_{i(t)}[G_{i(t)}]$ . We assume that the captured RGB-D images have been segmented into foreground objects and background. We discard all color details and only retain the depth information. We further extract the heightmap of container  $H_c$  with resolution  $\lceil S_x/\Delta_h \rceil \times \lceil S_y/\Delta_h \rceil$ , where  $\Delta_h$  is a regular interval. And we get a surface point cloud  $P$  belonging to  $T_{i(t)}[G_{i(t)}]$ . We thus define our observation function as  $o(s_t) = (H_c, P)$ , which is also illustrated in Fig. 3ab.

*Action Space  $\mathcal{A}$ .* As mentioned in Section 3.1, the space for robot decision spans the entire  $\mathbb{R}^3 \times SO(1)$ , involving desired packing position and vertical orientation of the  $i(t)$ th object. We can naturally omit the  $z$ -dimension decision because of the top-down placement manner. Typically, a robotic hardware platform such as [Pan and Hauser 2021] is equipped with force sensors and can determine the opportune time for releasing an object once collisions are detected. Therefore, no height measurement is needed for the object. Similarly, once the bottom object surface and the container heightmap are captured, we can get the object’s landing altitude  $l_z$  when being placed at  $(l_x, l_y)$  coordinates [Wang and Hauser 2019] and we denote  $l_z$  as a function  $l_z(l_x, l_y)$ . Our packing policy only needs to figure out horizontal positions  $l_x, l_y$  for given vertical rotation  $\theta$ , essentially reducing the action space to  $SE(2) \times SO(1)$ . We define our action as  $a_t \triangleq (\theta, l_x, l_y, l_z)$ , where  $l_z$  is optional.

However, the  $SE(2) \times SO(1)$  space is still unaffordable for the sequential-decision nature of packing. For enabling efficient and effective policy learning, we propose to prune this enormous action space to limited placement candidates via a geometric-inspired method and use a parameterized policy to further select the best one. Our motivation and implementation of this candidate-based packing pattern will be deferred to Section 3.3.

*Reward Signal  $R$ .* Since we aim to maximize the packing utility in Equation 1, we directly grant a reward  $R(s_t, a_t) = w|G_{i(t)}|$  proportional to the volume of  $G_{i(t)}$  once  $G_{i(t)}$  is successfully placed inside the container. Here  $w$  is a constant weight. Otherwise, the reward is zero and the trajectory is terminated. To avoid premature trajectory termination and get more step-wise profits, the agent should learn to optimize the packing process for accommodating more future possible objects.

### 3.3 Candidate-Based Packing Pattern

In this section, we introduce our packing policy representation, including a theoretically-provable candidate action generation method and a learnable policy for further candidate selection.

*3.3.1 Candidate Action Generation.* An intuitive attempt for acting in the  $SE(2) \times SO(1)$  space is discretizing it using a regular interval, as done in [Goyal and Deng 2020]. However, this leads to a large action space which also grows exponentially with higher resolutions and larger container sizes. Meanwhile, the clustered actions with close distances also result in meaningless RL exploration. Generating an effective action subset with a controllable size is necessary for efficient packing policy learning which is also verified in [Zhao et al. 2022b] for cuboid packing.

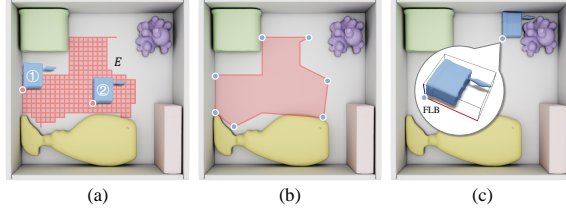


Fig. 6. We illustrate the procedure for generating candidate actions. Given an in-plane rotation of the object,  $\theta$ , we first extract feasible and connected action regions  $E$  for the incoming object. One found region is exemplified in (a). Assigning the incoming object to grid points inside ① or on the edge ② of this region would leave small gaps with less potential for accommodating future objects. We approximate the contour of this region to a polygon and detect convex polygon vertices (b). Our candidate actions correspond to having the FLB corner of the object’s AABB at a convex vertex (c) which makes the object placed tightly against the obstacles. This procedure is repeated once for each discretized rotation  $\theta$ .

Given an object to be packed, we hope to find a finite set of candidate actions leading to a tight packing of the object. Since we adopt a top-down placement manner, we are allowed to simplify the action space of object placement as a few connected 2D regions  $\mathcal{E} = \{E_i\}$ , each of which has a similar  $l_z$  value. Our general goal is to pack the object in one of the connected regions in a compact manner so that as much empty room as possible can be left for future object packing. See an illustration in Fig. 6a. To ensure compact packing, we conjecture that the object should be placed at a (locally) convex vertex of a connected region (Fig. 6b), with which we can obtain a set of the candidate placement of the object as the action space. To theoretically verify that, we prove the following theorem:

**THEOREM 3.1.** *For a (polygonal) connected region  $E$  and a point on its boundary  $p \in \partial E$ , if  $p$  is a convex vertex, then  $p = \arg \max_{p' \in \mathcal{N}(p)} \tau(p')$  for an open neighborhood  $\mathcal{N}(p)$  of  $p$  which does not contain any other convex vertices and a tightness measure  $\tau(\cdot)$ .*

We define the tightness measure as the range of directions making  $\{p\} \oplus G_{\theta(t)}$  touch the obstacles (container boundary or already placed objects) and permit no further movement, where  $\oplus$  is Minkowski sum [Mark et al. 2008] and we vertically rotate  $T_{i(t)}[G_{i(t)}]$  with  $\theta$  to get  $G_{\theta(t)}$ . See Fig. 7 for the explanation of this definition. We provide a proof of this theorem in Appendix A. Essentially, this theorem claims that a convex vertex of  $E$  is a *local optimum* that leads to a tight object packing (see Fig. 6c) which can be chosen as an action of the candidate. This greatly reduces the action space and benefits RL-based policy learning.

Given a fixed in-plane rotation  $\theta$ , we construct the candidate action set for  $G_{\theta(t)}$  using three steps. We firstly consider placement positions  $F$  which satisfy  $F \oplus G_{\theta(t)} \subset C$  and  $F \oplus G_{\theta(t)} \cap \bar{T}_{i(t')}^{-1} G_{i(t')} = \emptyset$ , for  $t' < t$ . We discretize the container  $C$  into regular grids and sample grid points  $(l_x, l_y, l_z)$  lying in  $F$ . Next, we detect and cluster feasible, connected 2D regions  $E$  from discretized positions which result in  $G_{\theta(t)}$  placed with similar altitudes, see also Fig. 6a. We denote two neighboring grids  $(l_x, l_y)$  and  $(l'_x, l'_y)$  as connected if:

$$|l_z(l_x, l_y) - l_z(l'_x, l'_y)| \leq \Delta_z, \quad (3)$$

with  $\Delta_z$  being a constant parameter. As our third step, for each connected region  $E \in \mathcal{E}$ , we draw the region contour  $\partial E$  [Suzuki and Abe 1985] where  $\partial E \oplus G_{\theta(t)}$  touches the container boundary or packed objects from the top-down view. Since contours  $\partial E$  are pixelized, we approximate  $\partial E$  to polygons with the Ramer-Douglas-Peucker algorithm [Ramer 1972] and detect convex polygon vertices as candidate FLBs (Fig. 6b). We execute this procedure for all possible in-plane rotations discretized at a regular interval of  $\Delta_\theta$ . Finally, the number of candidate FLB positions can be large, and we sort

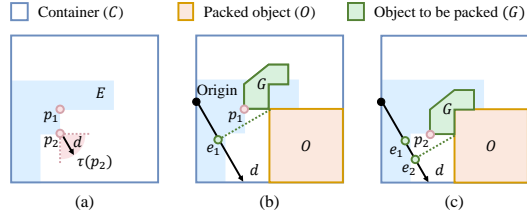


Fig. 7. Given a point  $p$  in the empty space represented by a polygon  $E$ , we define a tightness measure  $\tau(p, G)$  of packing  $G$  at  $p$  as the range of directions  $d$  along which the extreme value of  $G$ 's projection, i.e.,  $e(G, p, d) = \max_{g \in \{p\} \oplus G} (d^T g)$ , reaches a local maximal over a neighborhood of  $p$ :  $p = \arg \max_{q \in N(p)} e(G, q, d)$ . This means that  $G$  is tightly packed against obstacles at  $p$  along  $d$ . In (a), the range for point  $p_2$  is depicted as the pink sector. For  $p_1$  which is a concave vertex,  $e_1 = e(G, p_1, d)$  is not locally maximal since there are points nearby like  $p_2$  which has a larger extreme value  $e_2 > e_1$ . In fact, there does not exist a direction along which  $e_1$  can attain local maximal, so  $\tau(p_1) = 0$ . For the convex vertex  $p_2$ , however,  $\tau(p_2) = \pi/2$  corresponding to the pink sector in (a).

---

**ALGORITHM 1:** Candidate Action Generation
 

---

- 1: Sample  $\theta$  at a regular interval  $\Delta_\theta$
  - 2: Sample points  $(l_x, l_y)$  from  $H_c$  per  $\Delta_g$  grids
  - 3: **for** each sampled  $\theta$  **do**
  - 4:   **for** each grid point  $(l_x, l_y)$  **do**
  - 5:     Compute  $l_z(l_x, l_y)$
  - 6:     Rewrite infeasible  $l_z(l_x, l_y) = \infty$
  - 7:   **for** each pair of grid points  $(l_x, l_y)$  and  $(l'_x, l'_y)$  of  $H_c$  **do**
  - 8:     Connect neighbors if Equation 3 holds
  - 9:     Candidate action set  $A \leftarrow \emptyset$
  - 10:     Detect connected regions
  - 11:    **for** each connected region **do**
  - 12:     Draw the region contour and approximate it as a polygon
  - 13:     Detect convex polygon vertices and insert them into  $A$
  - 14:     Sort  $A$  by  $l_z(l_x, l_y)$  and retain the first  $N$
- 

them by  $l_z(l_x, l_y)$  in ascending order and retain the first  $N$ . We outline the candidate generation details in Algorithm 1. Our candidate generation procedure imposes no requirement on object geometry and fits the general shape packing need.

**3.3.2 Policy Parameterization.** Given the packing observation tuple  $(H_c, P)$  and the generated candidate actions, our packing policy  $\pi(o(s_t), \omega)$  is used to understand 3D task geometry and rank candidates for selection. Our policy first encodes the container heightmap  $H_c$  by a Convolutional Neural Network (CNN) to extract feature  $f_h$ . Similarly, we use a PointNet architecture [Qi et al. 2017] to project the point cloud  $P$  to feature  $f_p$ . Both feature extractors are designed lightweight for faster training. We apply a vertical transform to the point cloud until its AABB has the smallest volume with FLB at the origin. This essentially follows a similar idea to [Zeng et al. 2020] which transforms the point cloud to a canonical pose to improve data efficiency. The  $i$ th candidate action is brought through an element-wise Multi-Layer Perceptron (MLP) to derive a candidate descriptor  $f_a^i$ . Our candidate selector then takes the same form as a standard dueling Q-network [Wang et al. 2016], which is also illustrated in Fig. 3. This architecture represents the state-action value function  $Q(s, a)$  as:

$$Q(s_t, a_i) = V(s_t) + A(s_t, a_i)$$

where  $N$  is the number of candidate actions.  $V(s_t)$  is called the state value function and  $A(s_t, a_i)$  is the advantage function. We concatenate and parameterize the problem features to  $V$  and  $A$  with two MLPs, with learnable parameters  $\alpha$  and  $\beta$ , respectively:

$$\begin{aligned} V(s_t) &= \text{MLP}(f_h, f_p, \alpha), \\ A(s_t, a_i) &= \text{MLP}(f_h, f_p, f_a^i, \beta). \end{aligned}$$

Our ultimate action is defined as:

$$a_t \triangleq \operatorname{argmax}_{a_i} Q(s_t, a_i).$$

The number of candidate actions accepted by our policy is fixed to  $N$ . If the factual number of candidates is less than  $N$ , we fulfill the candidate array with dummy actions that are all-zero tuples. The Q-value predictions for these redundant candidates are replaced with  $-\infty$  during action selection.

### 3.4 Asynchronous Policy Training in Simulation World

Aside from that the complex irregular geometry and imperfect object placement enlarge the combinatorial solution space of packing, the heavy cost of exploring this enormous solution space, i.e. physics simulation, also makes it more difficult to learn an effective packing policy. In this section, we discuss several practical approaches to improve the efficiency of exploration and policy training in the simulation world. We choose a data-efficient off-policy RL algorithm and further use an asynchronous pipeline for accelerating the training, where the simulation-intensive trajectory sampling and policy optimization are performed asynchronously; a partial simulation further lowers the sample cost.

Existing reinforcement learning algorithms can be largely divided into on-policy approaches [Schulman et al. 2017; Wu et al. 2017] and off-policy methods [Barth-Maron et al. 2018; Wang et al. 2016]. The former maximizes the expectation in Equation 2 by sampling trajectories using the current policy, while the latter maintains an experience memory  $D$  that stores trajectories sampled using out-of-sync policies. Off-policy methods minimize the Bellman loss using samples from  $D$ :

$$\operatorname{argmin}_{\omega} \mathbb{E}_{(s,a,r,s') \sim D} \left[ (r + \gamma \max_{a'} Q(s', a') - Q(s, a))^2 \right].$$

The ability to reuse samples makes off-policy algorithms more data-efficient, which is critical to our problem. As mentioned in Section 3.3, we use dueling networks [Wang et al. 2016] to allow more frequent updates of  $V(s)$  and share the learning across multiple candidate actions. We adopt the discrete action space DRL algorithm — Rainbow [Hessel et al. 2018] to train the dueling networks. Besides the dueling architecture, the Rainbow algorithm also fruitfully combines the well-known DQN method [Mnih et al. 2015] with other five independent improvements like prioritized replay [Schaul et al. 2016], noisy nets [Fortunato et al. 2018], distributional Q-learning [Bellemare et al. 2017], and so on.

**3.4.1 Asynchronous Rainbow.** In the vanilla Rainbow algorithm, the experience collection step and the policy learning step run alternatively, as demonstrated in Fig. 8a. For our problem, however, experience collection via physics simulation is CPU-bound and time-consuming, which leaves policies less trained. Given that the policy learning is merely GPU-bound, we propose to parallelize training via an asynchronous scheme similar to [Horgan et al. 2018]. Specifically, we create an actor and a learner residing in two different processes, as illustrated in Fig. 8b. The actor interacts with the

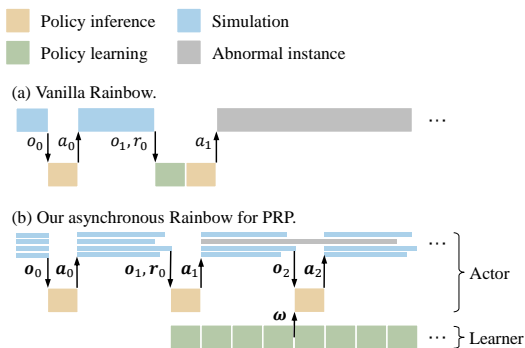


Fig. 8. The vanilla Rainbow flowchart (a) and that of our asynchronous version (b). The vanilla Rainbow (a) runs the CPU-bound physics simulations and GPU-bound policy optimization in a sequential manner, which leads to idle computing resources and under-trained policies. This also results in the uniform training schedule being blocked when an abnormal instance (gray) is sampled. Instead, our method (b) runs an experience sampling actor and a policy learner in asynchronous processes. The experience sampling is performed on a batch of CPU threads. The learner keeps learning on GPU and shares the updated policy parameter  $\omega$  with the actor. The batch of threads is synchronized when policy inference is needed. We further incorporate an abnormal detection mechanism, so that the abnormal thread is not synchronized with other normal ones.

packing environment and collects experience. The collected data is saved to a memory  $D$  which is shared between processes. The learner keeps learning from  $D$  and spontaneously updates the actor with the latest parameters. Our asynchronous implementation not only saves wall-clock training time but also accesses higher-quality experiences by having the actor refine its parameter more frequently before each decision.

To further accelerate the experience collection step, we run multiple simulation threads along with a non-blocking treatment in the actor process. There are two-fold benefits of doing so. First, more sampling threads enrich experiences for policy learning. Moreover, the batched simulation also avoids the uniform training schedule being blocked by abnormally slow instances, as exemplified in Fig. 8a. Such abnormality can happen when the physical simulator is unstable and experiences a sudden gain in kinetic energy, requiring many more timesteps to converge to a new equilibrium configuration. We suspend the actor thread whenever its reaction time is longer than a threshold, as demonstrated in Fig. 8b. This suspended thread will then be treated as a standalone instance and rejoin others after its task is finished. This implementation guarantees sufficient concurrency in trajectory sampling.

**3.4.2 Partial Simulation.** Even by using asynchronous Rainbow, the policy training for PRP is still bound by the massive simulation cost. We can further accelerate training by fixing the configurations of already packed objects. In practice, we find that old objects are not affected much by new arrivals. Using this strategy can save a large portion of simulation costs. It can also save the price of computing heightmap  $H_c$ , since we only need to update the slice of  $H_c$  covered by the newly arrived object  $\tilde{T}_{i(t)}^t [G_{i(t)}]$  but scan the entire container. This simple strategy can significantly boost the simulation frequency by more than three times. Note that this partial simulation is only used during training, and we always simulate all objects and scan the entire container at test time for practicality.

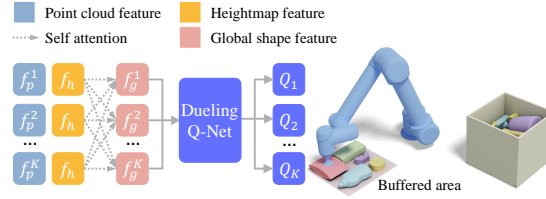


Fig. 9. (a): Our object-ordering policy, consisting of a Graph Attention Network (GAT) and a dueling Q-Network ranker. (b): The robot picks the object with the highest Q-value from the buffer and packs it into the container.

### 3.5 Extension to Buffered Packing Scenario

So far we have discussed the strictly online packing problem. In some real-world scenarios, a buffered area  $B$  can be used to temporarily store objects before the final placement, as shown in Fig. 9. By introducing the buffer, the robot can reorder objects locally before packing, potentially improving the packing performance by enabling a much larger search space. We suppose the buffered area is of a fixed size  $K$ . When a new object comes, the robot will store this object in  $B$ . If there are already  $K$  objects inside  $B$ , the robot will pass on one of the objects from  $B$  to  $C$ . Solving this problem not only involves reasoning about the picked object geometry, but considering the permutation of objects inside the buffer and future possible ones as well. To this end, we use an additional policy  $\pi_s$  to select objects from  $B$ , which is followed by our packing policy  $\pi$  in Section 3.2. The area of  $B$  is sufficiently large such that objects can be placed horizontally, and the point cloud feature of each object in  $B$  is stored and available to  $\pi_s$ . Finally, we assume the robot can reach any position in the buffered area from a top-down view.

Our architecture of  $\pi_s$  is illustrated in Fig. 9a. We assume there are  $K$  objects in the buffer, denoted as  $G_1, \dots, G_K$ , with their point clouds being  $P_1, \dots, P_K$ . Similar to Fig. 3, our policy  $\pi_s$  first maps each  $P_k$  to a feature  $f_p^k$  in an element-wise manner and maps the container heightmap  $H_c$  to a feature  $f_h$ . We adopt a Graph Attention Network (GAT) [Velickovic et al. 2018] to project the tuple  $(f_p^k, f_h)$  to a high-level element feature  $f_g^k$ . A dueling Q-network block is then used to select the best object with  $\text{argmax}_{k=1, \dots, K} Q(s_t, G_k)$ , where  $s_t$  is the average of all  $f_g$  features. We train the object-ordering policy  $\pi_s$  and the placement policy  $\pi$  jointly in an end-to-end manner. That is,  $\pi_s$  first chooses one shape  $G_k$ , then it is  $\pi$ 's turn to cooperate and choose a candidate action for placing  $G_k$ .

## 4 RESULTS AND EVALUATION

In this section, we first explain our packing experiment setup. Then, we describe our carefully prepared datasets emulating realistic packing tasks in Section 4.1. We illustrate the superiority of our method for online packing by comparing it with a row of existing baselines in Section 4.2 and demonstrate the benefits of our candidate-based packing pattern in Section 4.3. We report the generalization results of our method in Section 4.4, where the problem emitter transfers to noisy point cloud inputs and unseen shapes. Immediately following, we show performance on buffered packing scenarios in Section 4.5.

We establish our packing environment using the Bullet simulator [Coumans and Bai 2016], with a deep container of size  $S_x = 32\text{cm}$ ,  $S_y = 32\text{cm}$ , and  $S_z = 30\text{cm}$  following Wang and Hauser [2019]. We assume all objects have the same uniform density for estimating the center of mass. The coefficients of friction among objects and against the container are both set to 0.7. We set the grid size of the heightmap  $H_c$  to be  $\Delta_h = 1\text{cm}$ . We then sample  $H_c$  at an interval of  $\Delta_g = 2$  grids to form grid points for the candidate generation procedure. For clustering the connected region with similar  $l_z$

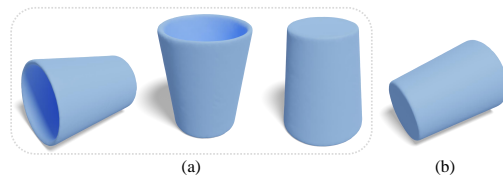


Fig. 10. (a): Different planar-stable poses of a bucket shape. These poses have invariant appearances after vertical rotations and we remove redundant poses (b) to avoid imbalanced shape distribution.

values, we use  $\Delta_z = 1\text{cm}$ . Unless otherwise stated, we use  $\Delta_\theta = \pi/4$  to discretize object rotations. We use a maximum of  $N = 500$  candidate actions for policy ranking. Our PointNet takes a fixed-sized set of 1024 points, so we resample 1024 points from the surface point cloud  $P$  to fit this size. We adopt 16 simulation threads in the actor process. Our learning-based policies are trained within 48 hours on a desktop computer equipped with a Xeon E5-2620 CPU and a TITAN Xp GPU. Ablations on these experimental parameters and training methods are reported in Appendix C.

#### 4.1 Object Data Preparation

For training reliable policies for packing irregular 3D shapes, we need to prepare object datasets that contain abundant shapes as well as their planar-stable poses, while being compatible with the simulator. Our object test suite combines objects from widely used, open-source polygonal mesh [Botsch et al. 2010] datasets, collected either by synthetic modeling or real-world scanning. To perform robust collision detections and ray-casting tests in the simulation world, we stipulate that objects are represented as closed manifold mesh surfaces. For each object, we first use the method in [Stutz and Geiger 2020] to reconstruct the mesh into a watertight one. We then extract all the planar-stable poses using the detection algorithm [Goldberg et al. 1999], as explained in Fig. 10a. Some planar-stable poses are rotation-symmetric as shown in Fig. 10b and we propose Algorithm 3 in Appendix B to remove redundant poses and retain only one representative from each rotation-symmetric group. This step avoids unbalanced shape distributions and improves the robustness of trained policies.

Finally, several rigid body simulators only accept convex shape primitives, e.g., approximating a non-convex power drill shape with its convex hull in Fig. 11a (red). We thus apply the convex decomposition algorithm [Mamou et al. 2016] for non-convex shapes, as illustrated in Fig. 11b. The complete data preparation pipeline is outlined in Algorithm 2 of Appendix B. The packing result or the final packing utility is highly related to the geometric properties of the picked object dataset. For providing convincing evaluations, we apply our pipeline to construct three datasets of various features.

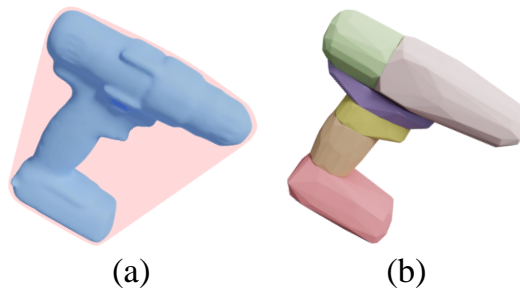


Fig. 11. Convex decomposition.

**General** is a large dataset made up of daily life objects, as illustrated in Fig. 12a. It combines shapes from the KIT dataset [Kasper et al. 2012], the BigBIRD dataset [Singh et al. 2014], the GD dataset [Kappler et al. 2015], the APC dataset [Rennie et al. 2016], and the YCB dataset [Çalli et al. 2017], totaling 483 shapes and 1094 planar-stable poses. All these shapes are collected through real-world scanning. *General* is our main dataset for profiling the performance of different methods.

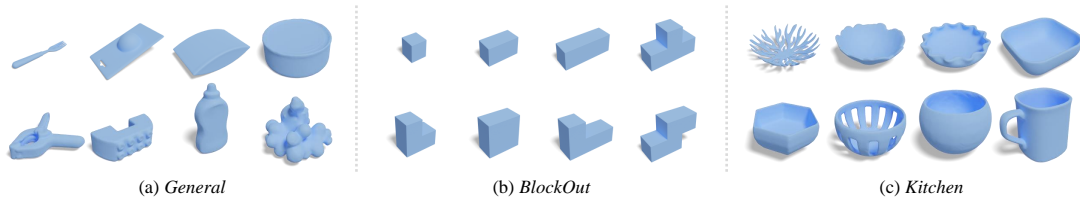


Fig. 12. Gallery of our datasets. (a): Part of shapes from the *General* dataset. (b): All polyominoes from the *BlockOut* dataset, where each polyomino is presented with a selected pose. (c): The bowl shapes from the *Kitchen* dataset. The shapes in (a) and (c) are scaled with their maximal AABB size equal to 1.

**BlockOut** is a synthetic 3D puzzle dataset with polyominoes that comes from Lo et al. [2009]. This dataset includes 8 polyominoes with 23 planar-stable poses, as illustrated in Fig. 12b. Each polyomino is composed of basic cubes of the same size. This dataset involves relatively regular shapes that are more complex to handle than cubical objects in BPP problems. *BlockOut* demonstrates the algorithm’s ability to understand shapes and combine them, as done in Fig. 2.

**Kitchen** consists of three categories of shapes, namely bowl, board, and fruit. The bowl shapes are concave CAD models collected from the ShapeNet dataset [Chang et al. 2015], as illustrated in Fig. 12c. The board shapes are manually created by us and the fruit shapes are small items coming from the *General* dataset. This dataset is created in order to verify a commonsense logic: an effective packing method would try to place fruits in bowls before covering boards. We expect the learned policies to pick up such logical rules without human intervention thus achieving better packing performance.

We compose the polyominoes in the *BlockOut* dataset with basic cubes with a side length of 6cm. Therefore, the upper packing utility bound for the chosen container is 87.9%. The rotation interval  $\Delta_\theta$  for *BlockOut* is set to  $\Delta_\theta = \pi/2$  since the polyomino shapes are axis-aligned. To construct the *Kitchen* dataset, we collect 54 concave bowl shapes from the ShapeNet dataset, 106 fruits from the *General* dataset, and 20 planar boards generated with random sizes. The problem emitter for the *Kitchen* dataset is slightly different from the others. Since we focus on verifying the packing logic between shape categories, we first sample an object category and then sample a random object with its most stable pose from this category. We also provide experimental results on industrial shapes collected from the ABC dataset [Koch et al. 2019] in Appendix C.

#### 4.2 Comparisons with Heuristic Baselines

We compare our learned policies with several representative heuristic methods that can pack irregular 3D shapes. The MTPE heuristic [Liu et al. 2015] searches for the pose of the lowest center-of-mass height. The HM heuristic [Wang and Hauser 2019] chooses to minimize the volume increase as observed from the top-down direction. The BLBF [Goyal and Deng 2020] heuristic chooses the bottom-most, left-most, and back-most placement. We also test a classic First-Fit (FF) [Falkenauer 1996] packing logic which places items in the first found feasible placement. We run all methods in the same environment setup with the same test sequences. Totalizing 2000 object sequences randomly generated from each dataset are tested. These baselines are compared along five different metrics. First, we have the packing utility in Equation 1 which is the volume of packed objects divided by the volume of  $C$ . Except for the *BlockOut* dataset which is composed of regular cubes, the optimal packing ground truths of other datasets are hard to obtain. Therefore, we



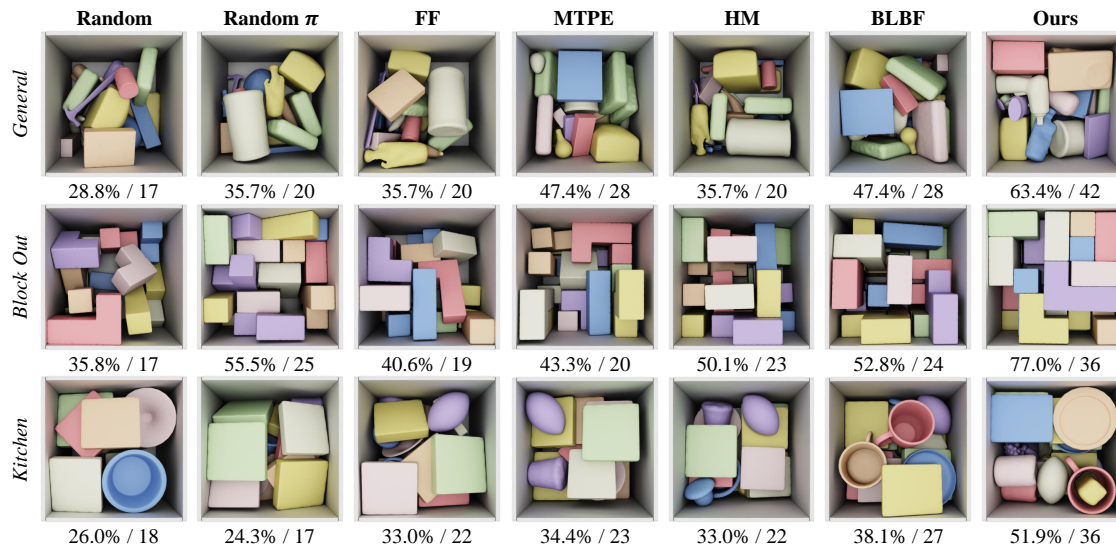


Fig. 13. Visualization of various packing methods on three datasets. Each test instance is labeled with its utility/number of packed objects. Our learned policy consistently exhibits tight packing and achieves the best performance.

Table 1. Online packing performance comparisons along five diverse metrics. From left to right: packing utility (Uti.), optimality gap (Gap), the variance of packing utility in units of  $10^{-3}$  (Var.), average number (Num.) of objects packed, and average decision-making time measured in seconds (Time). We also report statistics of two basic baselines where the agent randomly chooses placement from the resolution-complete action space (Random) and chooses candidate actions with a randomly initialized policy (Random  $\pi$ ).

Method	<i>General</i>					<i>BlockOut</i>					<i>Kitchen</i>				
	Uti.	Gap	Var.	Num.	Time	Uti.	Gap	Var.	Num.	Time	Uti.	Gap	Var.	Num.	Time
Random	31.6%	29.0%	5.8	19.6	0.03	37.1%	47.7%	3.4	17.8	0.02	22.6%	42.3%	6.4	16.7	0.03
Random $\pi$	32.9%	26.1%	4.6	20.4	0.04	42.1%	40.7%	3.5	20.2	0.02	25.8%	34.2%	5.5	18.9	0.03
FF [1996]	36.2%	18.7%	4.6	22.2	0.03	43.0%	39.4%	4.0	20.6	0.02	26.4%	32.7%	6.3	19.3	0.03
MTPE [2015]	37.3%	16.2%	4.6	22.7	0.04	58.4%	17.7%	3.6	27.9	0.02	32.2%	17.9%	5.1	23.4	0.03
HM [2019]	35.8%	19.6%	4.8	21.8	0.03	59.5%	16.2%	3.7	28.4	0.02	32.6%	16.8%	5.4	23.7	0.03
BLBF [2020]	36.6%	17.8%	4.6	22.7	<b>0.03</b>	61.9%	12.8%	4.1	29.5	0.02	32.0%	18.4%	5.2	23.3	0.03
Ours	<b>44.5%</b>	<b>0.0%</b>	<b>3.4</b>	<b>27.7</b>	0.04	<b>71.0%</b>	<b>0.0%</b>	<b>1.7</b>	<b>34.8</b>	<b>0.02</b>	<b>39.2%</b>	<b>0.0%</b>	<b>4.5</b>	<b>29.4</b>	<b>0.03</b>

provide the utility gap against the best baseline to highlight the performance discrepancy. We also list the utility variance and the average number of packed objects. Finally, we show the average time cost of each packing decision-making.

The quantitative and qualitative comparisons are summarized in Table 1 and Fig. 13, respectively. The best-performing heuristic for each dataset varies due to their distinct geometric properties. For example, MTPE has an advantage on the *General* dataset while HM is the best heuristic for *Kitchen* with more non-convex shapes. Compared to these manually designed packing rules, our learned policies adapt well to each dataset and consistently dominate heuristic rules. The gap metric demonstrates that our method outperforms even the best-performing baseline on each dataset with at least 12.8% in terms of packing utility. All these methods meet real-time packing requirements with a framerate of at

least 25. Our method also achieves the smallest variance on each dataset. More packing visualizations are provided in Appendix C. We also provide a dynamic packing video in the supplemental material.

### 4.3 Benefits of Candidate-based Packing Pattern

One of our main contributions lies in action space design, i.e., the candidate-based packing pattern for pruning sub-optimal actions. We highlight the effectiveness of our design in this section. We first compare with the resolution-complete action space, which discretizes the action space using a regular interval as done in [Goyal and Deng 2020]. This action space can also be treated as a full geometry set including convex vertices, concave vertices, edges, and internal points of connected action regions, which would demonstrate the functionality of our generated candidates. Then, we also compare with other dimension-reduction techniques below.

Table 2. Performance comparisons between various kinds of action space design along our five metrics.

Action Space Design	<i>General</i>					<i>BlockOut</i>					<i>Kitchen</i>				
	Uti.	Gap	Var.	Num.	Time	Uti.	Gap	Var.	Num.	Time	Uti.	Gap	Var.	Num.	Time
Resolution-Complete	41.6%	6.5%	5.0	26.4	0.04	55.7%	21.5%	3.4	27.7	0.02	32.7%	16.6%	5.2	25.5	0.03
Act in Line	42.2%	5.2%	4.4	26.8	<b>0.03</b>	60.3%	15.1%	2.7	29.9	0.02	34.9%	11.0%	<b>4.2</b>	27.1	0.03
Act on Orientation	38.6%	13.3%	5.2	24.6	0.03	57.6%	18.9%	3.6	28.5	0.02	32.1%	18.1%	5.6	25.1	0.03
Act on Heuristics	40.1%	9.9%	6.0	25.5	0.03	65.4%	7.9%	2.6	32.2	0.02	32.8%	16.3%	5.6	25.4	0.03
Ours	<b>44.5%</b>	<b>0.0%</b>	<b>3.4</b>	<b>27.7</b>	0.04	<b>71.0%</b>	<b>0.0%</b>	<b>1.7</b>	<b>34.8</b>	<b>0.02</b>	<b>39.2%</b>	<b>0.0%</b>	4.5	<b>29.4</b>	<b>0.03</b>

*Act in Line.* The resolution-complete action space for packing is typically large and sensitive to the container size  $S$  and the related intervals  $\Delta$  for discretizing the space  $SE(2) \times SO(1)$ . We can get the scale of this discretized space  $|\mathcal{A}| = O(S^2 \Delta^{-3})$ . To sidestep such an enormous space that can grow explosively, we only require the robot to provide  $l_x$  and  $\theta$ . The position  $l_y$  can be determined via  $\operatorname{argmin}_{l_y} l_z(l_x, l_y)$  for given  $\theta$ , thus reducing the action space to  $\mathbb{R} \times SO(1)$  with  $|\mathcal{A}| = O(S \Delta^{-2})$ .

*Act on Orientation.* Along the same line of thinking, we can further reduce the action space by only asking the robot to output  $\theta$  and determine  $l_x, l_y$  via  $\operatorname{argmin}_{l_x, l_y} l_z(l_x, l_y)$ . Thus reducing the action space to  $SO(1)$  with  $|\mathcal{A}| = O(\Delta^{-1})$ .

*Act on Heuristics.* Since heuristic methods have different packing preferences, a straightforward packing strategy is to select one of the heuristics for the object to be packed. We collect all heuristics mentioned in Section 4.2 as a candidate action set  $\mathbf{m}$ . The action space size, in this case, is  $|\mathcal{A}| = |\mathbf{m}|$ .

For all alternatives mentioned above, we replace Q-values of invalid actions with  $-\infty$  during decision-making, and performances are summarized in Table 2. The resolution-complete design, which is also a full geometry set of connected action regions, performs badly on each dataset. The reason is that a large action space must be trained with a huge amount of RL explorations, which is beyond regular computational capabilities. Benefits from dimension reduction, Act-in-Line achieves consistently better performance than resolution-complete actions. However, if we further reduce the action space to  $SO(1)$ , the decision flexibility decreases, and the performance of Act-on-Orientation degrades. Unsurprisingly, Act-on-Heuristics exceeds the performance of every single heuristic reported in Table 1. However, the

Table 3. The performance of our method when observation is corrupted by point cloud noises of different amplitude  $\sigma$ .

Noise	<i>General</i>			<i>BlockOut</i>			<i>Kitchen</i>		
	Uti.	Var.	Num.	Uti.	Var.	Num.	Uti.	Var.	Num.
$\sigma = 0$	44.5%	3.4	27.7	71.0%	1.7	34.8	39.2%	4.5	29.4
$\sigma = 1\%$	44.5%	3.5	27.7	70.7%	1.7	34.7	38.8%	4.5	29.0
$\sigma = 3\%$	44.4%	3.4	27.6	70.7%	1.7	34.7	38.9%	4.3	29.1
$\sigma = 5\%$	44.3%	3.4	27.6	70.5%	1.8	34.6	38.5%	4.5	28.9
$\sigma = 10\%$	43.6%	3.6	27.2	70.4%	1.7	34.6	37.3%	48.2	28.1

Table 4. Performance of our method trained with partial object datasets. We also provide test results from randomly initialized policies as a baseline.

Train	Test	<i>General</i>			<i>BlockOut</i>			<i>Kitchen</i>		
		Uti.	Var.	Num.	Uti.	Var.	Num.	Uti.	Var.	Num.
-	Full	32.9%	4.6	20.4	42.1%	3.5	20.2	25.8%	5.5	18.9
Full	Full	44.5%	3.4	27.7	71.0%	1.7	34.8	39.2%	4.5	29.4
Part	Full	44.3%	3.5	27.6	70.7%	1.4	34.7	39.1%	4.5	29.2

packing behavior of the learned policy is still restricted by basic heuristic components and the improvements are limited. In comparison, our method stands out as the consistently best performer by reducing the action space to candidate actions of a fixed size  $N$ , which both loosens the learning burden and enables tight object packing.

#### 4.4 Generalization Ability

The generalization of learning-based methods, i.e., testing the trained policies with a problem emitter different from the training one, has always been a concern. Here we demonstrate our generalization ability with two experiments from a practical perspective.

*Generalization on Noisy Point Clouds.* The point cloud used to represent the incoming object is re-sampled from  $P$  randomly. To demonstrate our generalizability, we apply Gaussian noises  $d \cdot N(0, \sigma^2)$  to the re-sampled  $P$ . Here  $\sigma$  is the standard deviation and  $d$  is the diagonal length of  $P$ 's AABB. Then we generalize the policies trained on  $\sigma = 0$  to  $\sigma = 1\% - 10\%$ .

*Generalization on Unseen Shapes.* To test our method on unseen shapes, we randomly remove 20% of shapes from each dataset for training and we test trained policies with full datasets. For the *Kitchen* dataset, this shape removal is performed by each category.

The generalization results on noisy point clouds and unseen shapes are summarized in Table 3 and Table 4 respectively. Our method maintains its performance under various amplitude of point cloud noises and behaves well even with a strong noise disturbance of  $\sigma = 10\%$ . The policies trained with only part of each dataset can still be well adapted to the full dataset, with a marginal drop in performance. Note that, even the worst generalization performance in Table 3 and Table 4 still clearly outperforms the best heuristic performance as reported in Table 1, which demonstrates the

Table 5. The buffered packing problem can be well solved by training an additional object-ordering policy  $\pi_s$  cooperating with the placement policy  $\pi$ . The online case with  $K = 1$  can be treated as a baseline, where no object-ordering policy exists and the objects are randomly dispatched.

Train	Test	Method	General					BlockOut					Kitchen				
			Uti.	Gap	Var.	Num.	Time	Uti.	Gap	Var.	Num.	Time	Uti.	Gap	Var.	Num.	Time
$K = 1$	$K = 1$	$\pi$	44.5%	-	3.4	27.7	0.04	71.0%	-	1.7	34.8	0.02	39.2%	-	4.5	29.4	0.03
$K = 10$	$K = 3$	LFSS & $\pi$	44.3%	2.2%	3.5	25.8	0.07	70.8%	1.3%	<b>1.5</b>	33.4	0.04	39.7%	10.4%	<b>4.7</b>	28.3	0.06
		$\pi_s$ & BLBF	42.0%	7.3%	3.9	27.8	<b>0.03</b>	66.9%	6.7%	2.7	33.2	<b>0.02</b>	38.1%	14.0%	4.8	29.5	<b>0.03</b>
		$\pi_s$ & $\pi$	<b>45.3%</b>	<b>0.0%</b>	<b>3.4</b>	<b>28.9</b>	0.07	<b>71.7%</b>	<b>0.0%</b>	2.4	<b>35.5</b>	0.04	<b>44.3%</b>	<b>0.0%</b>	5.5	<b>34.1</b>	0.07
$K = 10$	$K = 5$	LFSS & $\pi$	44.4%	6.5%	3.6	24.1	0.07	70.5%	5.7%	1.5	32.1	0.04	40.1%	17.8%	<b>4.9</b>	27.4	0.06
		$\pi_s$ & BLBF	45.3%	4.6%	4.1	30.3	<b>0.04</b>	70.9%	5.2%	2.1	35.3	<b>0.02</b>	42.3%	13.3%	5.0	32.9	<b>0.03</b>
		$\pi_s$ & $\pi$	<b>47.5%</b>	<b>0.0%</b>	<b>3.1</b>	<b>31.4</b>	0.07	<b>74.8%</b>	<b>0.0%</b>	<b>1.5</b>	<b>37.2</b>	0.05	<b>48.8%</b>	<b>0.0%</b>	5.5	<b>37.8</b>	0.07
$K = 10$	$K = 10$	LFSS & $\pi$	45.7%	18.0%	3.4	20.9	0.07	69.3%	11.2%	1.8	29.6	0.04	41.8%	27.7%	<b>5.6</b>	26.1	0.07
		$\pi_s$ & BLBF	49.6%	11.0%	4.0	32.9	<b>0.04</b>	74.8%	4.1%	2.0	36.9	<b>0.02</b>	50.5%	12.6%	5.9	38.7	<b>0.03</b>
		$\pi_s$ & $\pi$	<b>55.7%</b>	<b>0.0%</b>	<b>2.3</b>	<b>38.5</b>	0.07	<b>78.0%</b>	<b>0.0%</b>	<b>0.9</b>	<b>38.5</b>	0.05	<b>57.8%</b>	<b>0.0%</b>	6.4	<b>44.2</b>	0.07

robustness of our learned policies. We also conduct experiments to crossly test trained policies on other datasets, please see Section C.4.

#### 4.5 Performance on Buffered Packing Scenario

Here we show that our method can naturally solve the buffered packing problem by merely introducing an object-ordering policy  $\pi_s$  cooperating with the placement policy  $\pi$ . To verify that both  $\pi_s$  and  $\pi$  are necessary components, we compare them with the systematically corresponding heuristic baselines proposed by Goyal and Deng [2020]. Besides the placement heuristic BLBF mentioned above, Goyal and Deng [2020] also propose an LFSS method for ordering objects in a largest-volume-first preference. We combine LFSS with  $\pi$  and combine  $\pi_s$  with BLBF as our baselines. All learning-based policies are trained with buffer size  $K = 10$ . We further test the trained policies with various  $K$  to exemplify the generalization ability, as visualized in Fig. 14 and summarized in Table 5.

Our comparison shows that introducing an object-ordering policy  $\pi_s$  for buffered packing scenarios with  $K = 10$  significantly improves the packing performance compared with the strictly online case, where  $\pi_s$  does not exist and  $K = 1$ . The jointly trained policies  $\pi_s$  and  $\pi$  outperform the other two combination alternatives by a large margin on each dataset. This advantage was still well maintained when we generalize the trained policies to buffered packing scenarios with  $K = 3$  and  $K = 5$ . More packing results of our method on buffered packing are visualized in Appendix C.

To figure out what the two policies learned, we calculate the average volume of objects chosen by  $\pi_s$  during the packing process and visualize it in Fig. 15a. We can see that  $\pi_s$  automatically learns a strategy that selects objects from large to small like LFSS. We visualize a metric  $\sum |G_{i(t)}|/V_f$  in Fig. 15b to reflect space occupancy, where  $V_f$  is the volume below the up surface composed of packed objects. We can see that  $\pi_s$  can select more suitable items to keep higher occupancy than LFSS so that occupied space  $V_f$  is better utilized. Also, we can get that the learnable  $\pi$  also contributes better packing by comparing the occupancy between  $\pi_s + \text{BLBF}$  and  $\pi_s + \pi$ .

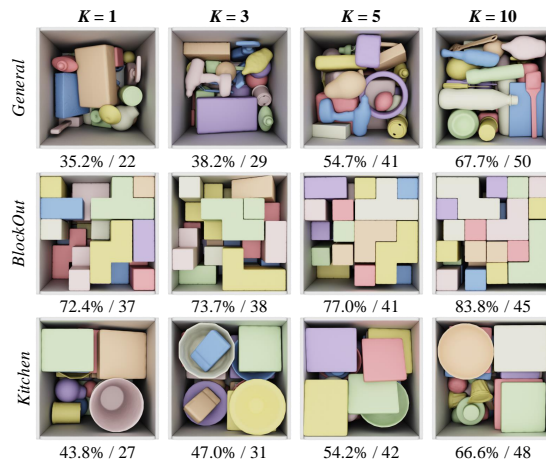


Fig. 14. Visualization results of our method on buffered packing scenarios with various  $K$ . The larger buffer provides more flexibility for the object-ordering policy  $\pi_s$  and results in a more dense packing.

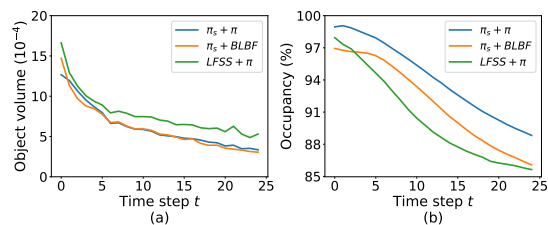


Fig. 15. Packing behavior analysis on the *General* dataset with  $K = 10$ . The policies  $\pi_s$  and  $\pi$  both contribute to better utilization of occupied spaces.

## 5 CONCLUSION AND FUTURE WORK

We investigate problem setups and solution techniques for learning online packing skills for irregular 3D shapes. We propose a learning-based method to successfully pack objects with complex 3D shapes at real-time rates, while taking physics dynamics and constraints of a placement into account. Our theoretically-provable candidate generation algorithm prunes sub-optimal actions and forms a set of placements for a learnable policy, leading to high-quality packing plans. Equipped with asynchronous RL acceleration techniques and a data preparation process of simulation-ready training sequences, a mature packing policy can be trained within 48 hours in a physically realistic environment.

Through evaluations on a variety of real-life object datasets, our performance beats state-of-the-art baselines in terms of both packing utilities and the number of packed objects. Our method can also be naturally extended to solve buffered packing problems by only introducing an additional object-ordering policy. Our results shed light on many other packing-related problems in the graphics community including UV generation and 3D printing. The limitation of this work is that we model the general irregular shapes as rigid bodies and neglect their material. For future research, we are interested in introducing the stress metric [Pan et al. 2020] for better placing fragile objects. Exploiting deformation during planning to achieve tighter packing [Yin et al. 2021] is also an interesting direction.

## REFERENCES

- Sara Ali, António Galvão Ramos, Maria Antónia Carravilla, and José Fernando Oliveira. 2022. On-line three-dimensional packing problems: a review of off-line and on-line solution approaches. *Computers & Industrial Engineering* (2022), 108122. <https://doi.org/10.1016/j.cie.2022.108122>
- Gabriel Barth-Maron, Matthew W. Hoffman, David Budden, Will Dabney, Dan Horgan, Dhruva TB, Alistair Muldal, Nicolas Heess, and Timothy P. Lillicrap. 2018. Distributed Distributional Deterministic Policy Gradients. In *6th International Conference on Learning Representations, ICLR 2018, Vancouver, BC, Canada, April 30 - May 3, 2018, Conference Track Proceedings*. OpenReview.net, Vancouver Convention Center, Vancouver Canada. <https://openreview.net/forum?id=SyZipzCb>
- Marc G. Bellemare, Will Dabney, and Rémi Munos. 2017. A Distributional Perspective on Reinforcement Learning. In *Proceedings of the 34th International Conference on Machine Learning, ICML 2017, Sydney, NSW, Australia, 6-11 August 2017 (Proceedings of Machine Learning Research, Vol. 70)*, Doina Precup and Yee Whye Teh (Eds.). PMLR, 449–458. <http://proceedings.mlr.press/v70/bellemare17a.html>
- Mario Botsch, Leif Kobbelt, Mark Pauly, Pierre Alliez, and Bruno Lévy. 2010. *Polygon Mesh Processing*. A K Peters. <http://www.crcpress.com/product/isbn/9781568814261>
- Stephen Boyd, Stephen P Boyd, and Lieven Vandenbergh. 2004. *Convex optimization*. Cambridge university press.
- Greg Brockman, Vicki Cheung, Ludwig Pettersson, Jonas Schneider, John Schulman, Jie Tang, and Wojciech Zaremba. 2016. OpenAI Gym. *CoRR abs/1606.01540* (2016). arXiv:1606.01540 <http://arxiv.org/abs/1606.01540>
- Berk Çalli, Arjun Singh, James Bruce, Aaron Walsman, Kurt Konolige, Siddhartha S. Srinivasa, Pieter Abbeel, and Aaron M. Dollar. 2017. Yale-CMU-Berkeley dataset for robotic manipulation research. *The International Journal of Robotics Research* 36, 3 (2017), 261–268. <https://doi.org/10.1177/0278364917700714>
- Angel X. Chang, Thomas A. Funkhouser, Leonidas J. Guibas, Pat Hanrahan, Qi-Xing Huang, Zimo Li, Silvio Savarese, Manolis Savva, Shuran Song, Hao Su, Jianxiong Xiao, Li Yi, and Fisher Yu. 2015. ShapeNet: An Information-Rich 3D Model Repository. *CoRR abs/1512.03012* (2015). arXiv:1512.03012 <http://arxiv.org/abs/1512.03012>
- Rulin Chen, Ziqi Wang, Peng Song, and Bernd Bickel. 2022. Computational Design of High-level Interlocking Puzzles. *ACM Transactions on Graphics (SIGGRAPH 2022)* 41, 4 (2022), 150:1 – 150:15. <https://doi.org/10.1145/3528223.3530071>
- Xuelin Chen, Hao Zhang, Jinjie Lin, Ruizhen Hu, Lin Lu, Qi-Xing Huang, Bedrich Benes, Daniel Cohen-Or, and Baoquan Chen. 2015. Dapper: decompose-and-pack for 3D printing. *ACM Transactions on Graphics (TOG)* 34, 6 (2015), 213:1–213:12. <https://doi.org/10.1145/2816795.2818087>
- John H Conway and Salvatore Torquato. 2006. Packing, tiling, and covering with tetrahedra. *Proceedings of the National Academy of Sciences* 103, 28 (2006), 10612–10617.
- Erwin Coumans and Yunfei Bai. 2016. Pybullet, a python module for physics simulation for games, robotics and machine learning. (2016).
- Lu Duan, Haoyuan Hu, Yu Qian, Yu Gong, Xiaodong Zhang, Jiangwen Wei, and Yinghui Xu. 2019. A Multi-task Selected Learning Approach for Solving 3D Flexible Bin Packing Problem. In *Proceedings of the 18th International Conference on Autonomous Agents and MultiAgent Systems, AAMAS '19, Montreal, QC, Canada, May 13-17, 2019*, Edith Elkind, Manuela Veloso, Noa Agmon, and Matthew E. Taylor (Eds.). International Foundation for Autonomous Agents and Multiagent Systems, 1386–1394. <http://dl.acm.org/citation.cfm?id=3331847>
- Yan Duan, Xi Chen, Rein Houthoofd, John Schulman, and Pieter Abbeel. 2016. Benchmarking deep reinforcement learning for continuous control. In *International conference on machine learning*. PMLR, 1329–1338. <http://proceedings.mlr.press/v48/duan16.html>
- Emanuel Falkenauer. 1996. A hybrid grouping genetic algorithm for bin packing. *Journal of heuristics* 2, 1 (1996), 5–30. <https://doi.org/10.1007/BF00226291>
- Meire Fortunato, Mohammad Gheshlaghi Azar, Bilal Piot, Jacob Menick, Matteo Hessel, Ian Osband, Alex Graves, Volodymyr Mnih, Rémi Munos, Demis Hassabis, Olivier Pietquin, Charles Blundell, and Shane Legg. 2018. Noisy Networks For Exploration. In *6th International Conference on Learning Representations, ICLR 2018, Vancouver, BC, Canada, April 30 - May 3, 2018, Conference Track Proceedings*. OpenReview.net. <https://openreview.net/forum?id=rywHCPkAW>
- Ken Goldberg, Brian Mirtich, Yan Zhuang, John Craig, Brian Carlisle, and John F. Canny. 1999. Part pose statistics: estimators and experiments. *IEEE Transactions on Robotics and Automation* 15, 5 (1999), 849–857. <https://doi.org/10.1109/70.795790>
- Ankit Goyal and Jia Deng. 2020. PackIt: A Virtual Environment for Geometric Planning. In *Proceedings of the 37th International Conference on Machine Learning, ICML 2020, 13-18 July 2020, Virtual Event (Proceedings of Machine Learning Research, Vol. 119)*. PMLR, 3700–3710. <http://proceedings.mlr.press/v119/goyal20b.html>
- Chi Trung Ha, Trung Thanh Nguyen, Lam Thu Bui, and Ran Wang. 2017. An Online Packing Heuristic for the Three-Dimensional Container Loading Problem in Dynamic Environments and the Physical Internet. In *Applications of Evolutionary Computation - 20th European Conference, EvoApplications 2017, Amsterdam, The Netherlands, April 19-21, 2017, Proceedings, Part II (Lecture Notes in Computer Science, Vol. 10200)*. 140–155. [https://doi.org/10.1007/978-3-319-55792-2\\_10](https://doi.org/10.1007/978-3-319-55792-2_10)
- Thomas Hales, Mark Adams, Gertrud Bauer, Tat Dat Dang, John Harrison, Hoang Le Truong, Cezary Kaliszzyk, Victor Magron, Sean McLaughlin, Tat Thang Nguyen, et al. 2017. A formal proof of the Kepler conjecture. In *Forum of mathematics, Pi*, Vol. 5. Cambridge University Press.
- Shuai D Han, Si Wei Feng, and Jingjin Yu. 2019. Toward fast and optimal robotic pick-and-place on a moving conveyor. *IEEE Robotics and Automation Letters* 5, 2 (2019), 446–453. <https://doi.org/10.1109/LRA.2019.2961605>
- Juris Hartmanis. 1982. Computers and intractability: a guide to the theory of np-completeness (michael r. garey and david s. johnson). *Siam Review* 24, 1 (1982), 90.

- Matteo Hessel, Joseph Modayil, Hado van Hasselt, Tom Schaul, Georg Ostrovski, Will Dabney, Dan Horgan, Bilal Piot, Mohammad Gheshlaghi Azar, and David Silver. 2018. Rainbow: Combining Improvements in Deep Reinforcement Learning. In *Proceedings of the Thirty-Second AAAI Conference on Artificial Intelligence, (AAAI-18), New Orleans, Louisiana, USA, February 2-7, 2018*, Sheila A. McIlraith and Kilian Q. Weinberger (Eds.). AAAI Press, 3215–3222. <https://www.aaai.org/ocs/index.php/AAAI/AAAI18/paper/view/17204>
- Dan Horgan, John Quan, David Budden, Gabriel Barth-Marón, Matteo Hessel, Hado van Hasselt, and David Silver. 2018. Distributed Prioritized Experience Replay. In *6th International Conference on Learning Representations, ICLR 2018, Vancouver, BC, Canada, April 30 - May 3, 2018, Conference Track Proceedings*. OpenReview.net. <https://openreview.net/forum?id=H1Dy--0Z>
- Haoyuan Hu, Xiaodong Zhang, Xiaowei Yan, Longfei Wang, and Yinghui Xu. 2017. Solving a New 3D Bin Packing Problem with Deep Reinforcement Learning Method. *CoRR* abs/1708.05930 (2017). arXiv:1708.05930 <http://arxiv.org/abs/1708.05930>
- Ruizhen Hu, Juzhan Xu, Bin Chen, Minglun Gong, Hao Zhang, and Hui Huang. 2020. TAP-Net: transport-and-pack using reinforcement learning. *ACM Transactions on Graphics (TOG)* 39, 6 (2020), 232:1–232:15. <https://doi.org/10.1145/3414685.3417796>
- Haojie Huang, Dian Wang, Robin Walters, and Robert Platt. 2022. Equivariant Transporter Network. *Proceedings of Robotics: Science and Systems (RSS)* (2022).
- Josef Kallrath. 2017. Packing ellipsoids into volume-minimizing rectangular boxes. *J. Glob. Optim.* 67, 1-2 (2017), 151–185. <https://doi.org/10.1007/s10898-015-0348-6>
- Daniel Kappler, Jeannette Bohg, and Stefan Schaal. 2015. Leveraging big data for grasp planning. In *IEEE International Conference on Robotics and Automation, ICRA 2015, Seattle, WA, USA, 26-30 May, 2015*. IEEE, 4304–4311. <https://doi.org/10.1109/ICRA.2015.7139793>
- Korhan Karabulut and Mustafa Murat Inceoglu. 2004. A Hybrid Genetic Algorithm for Packing in 3D with Deepest Bottom Left with Fill Method. In *Advances in Information Systems, Third International Conference, ADVIS 2004, Izmir, Turkey, October 20-22, 2004, Proceedings (Lecture Notes in Computer Science, Vol. 3261)*, Tatyana M. Yakhno (Ed.). Springer, 441–450. [https://doi.org/10.1007/978-3-540-30198-1\\_45](https://doi.org/10.1007/978-3-540-30198-1_45)
- Alexander Kasper, Zhixing Xue, and Rüdiger Dillmann. 2012. The KIT object models database: An object model database for object recognition, localization and manipulation in service robotics. *The International Journal of Robotics Research* 31, 8 (2012), 927–934. <https://doi.org/10.1177/0278364912445831>
- Sebastian Koch, Albert Matveev, Zhongshi Jiang, Francis Williams, Alexey Artemov, Evgeny Burnaev, Marc Alexa, Denis Zorin, and Daniele Panozzo. 2019. ABC: A Big CAD Model Dataset for Geometric Deep Learning. In *IEEE Conference on Computer Vision and Pattern Recognition, CVPR 2019, Long Beach, CA, USA, June 16-20, 2019*. Computer Vision Foundation / IEEE, 9601–9611. <https://doi.org/10.1109/CVPR.2019.00983>
- Bruno Lévy, Sylvain Petitjean, Nicolas Ray, and Jérôme Maillot. 2002. Least squares conformal maps for automatic texture atlas generation. *ACM Transactions on Graphics (TOG)* 21, 3 (2002), 362–371. <https://doi.org/10.1145/566654.566590>
- Max Limper, Nicholas Vining, and Alla Sheffer. 2018. Box cutter: atlas refinement for efficient packing via void elimination. *ACM Transactions on Graphics (TOG)* 37, 4 (2018), 153. <https://doi.org/10.1145/3197517.3201328>
- Hao-Yu Liu, Xiao-Ming Fu, Chunyang Ye, Shuangming Chai, and Ligang Liu. 2019. Atlas refinement with bounded packing efficiency. *ACM Transactions on Graphics (SIGGRAPH)* 38, 4 (2019), 33:1–33:13. <https://doi.org/10.1145/3306346.3323001>
- Xiao Liu, Jia-min Liu, An-xi Cao, and Zhuang-le Yao. 2015. HAPE3D - a new constructive algorithm for the 3D irregular packing problem. *Frontiers of Information Technology & Electronic Engineering* 16, 5 (2015), 380–390. <https://doi.org/10.1631/FITEE.1400421>
- Kui-Yip Lo, Chi-Wing Fu, and Hongwei Li. 2009. 3D polyomino puzzle. *ACM Transactions on Graphics (TOG)* 28, 5 (2009), 157. <https://doi.org/10.1145/1618452.1618503>
- Andrea Lodi, Silvano Martello, and Michele Monaci. 2002. Two-dimensional packing problems: A survey. *European journal of operational research* 141, 2 (2002), 241–252. [https://doi.org/10.1016/S0377-2217\(02\)00123-6](https://doi.org/10.1016/S0377-2217(02)00123-6)
- Linjie Luo, Ilya Baran, Szymon Rusinkiewicz, and Wojciech Matusik. 2012. Chopper: Partitioning models into 3D-printable parts. *ACM Transactions on Graphics (TOG)* 31, 6 (2012), 1–9. <https://doi.org/10.1145/2366145.2366148>
- Y. Ma, Zhonggui Chen, W. Hu, and W. Wang. 2018. Packing Irregular Objects in 3D Space via Hybrid Optimization. *Computer Graphics Forum* 37, 5 (2018), 49–59. <https://doi.org/10.1111/cgf.13490>
- Jeffrey Mahler and Ken Goldberg. 2017. Learning Deep Policies for Robot Bin Picking by Simulating Robust Grasping Sequences. In *1st Annual Conference on Robot Learning, CoRL 2017, Mountain View, California, USA, November 13-15, 2017, Proceedings (Proceedings of Machine Learning Research, Vol. 78)*. PMLR, 515–524. <http://proceedings.mlr.press/v78/mahler17a.html>
- Jeffrey Mahler, Florian T. Pokorny, Brian Hou, Melrose Roderick, Michael Laskey, Mathieu Aubry, Kai Kohlhoff, Torsten Kröger, James J. Kuffner, and Ken Goldberg. 2016. Dex-Net 1.0: A cloud-based network of 3D objects for robust grasp planning using a Multi-Armed Bandit model with correlated rewards. In *2016 IEEE International Conference on Robotics and Automation, ICRA 2016, Stockholm, Sweden, May 16-21, 2016*, Danica Kragic, Antonio Bicchi, and Alessandro De Luca (Eds.). IEEE, 1957–1964. <https://doi.org/10.1109/ICRA.2016.7487342>
- Khaled Mamou, E Lengyel, and A Peters. 2016. Volumetric hierarchical approximate convex decomposition. In *Game Engine Gems 3*. AK Peters, 141–158.
- de Berg Mark, Cheong Otfried, van Kreveld Marc, and Overmars Mark. 2008. *Computational geometry algorithms and applications*. Springer.
- Silvano Martello, David Pisinger, and Daniele Vigo. 2000. The Three-Dimensional Bin Packing Problem. *Operations research* 48, 2 (2000), 256–267. <https://doi.org/10.1287/opre.48.2.256.12386>
- Volodymyr Mnih, Koray Kavukcuoglu, David Silver, Andrei A. Rusu, Joel Veness, Marc G. Bellemare, Alex Graves, Martin A. Riedmiller, Andreas Fidjeland, Georg Ostrovski, Stig Petersen, Charles Beattie, Amir Sadik, Ioannis Antonoglou, Helen King, Dharshan Kumaran, Daan Wierstra, Shane Legg, and Demis Hassabis. 2015. Human-level control through deep reinforcement learning. *Nature* 518, 7540 (2015), 529–533. <https://doi.org/10.1038/nature14236>

- Tobias Nöll and D Stricker. 2011. Efficient packing of arbitrary shaped charts for automatic texture atlas generation. In *Computer Graphics Forum*, Vol. 30. Wiley Online Library, 1309–1317. <https://doi.org/10.1111/j.1467-8659.2011.01990.x>
- Zherong Pan, Xifeng Gao, and Dinesh Manocha. 2020. Grasping Fragile Objects Using A Stress-Minimization Metric. In *2020 IEEE International Conference on Robotics and Automation (ICRA)*. 517–523. <https://doi.org/10.1109/ICRA40945.2020.9196938>
- Zherong Pan and Kris Hauser. 2021. Decision Making in Joint Push-Grasp Action Space for Large-Scale Object Sorting. In *2021 IEEE International Conference on Robotics and Automation (ICRA)*. 6199–6205. <https://doi.org/10.1109/ICRA48506.2021.9560782>
- Charles Ruizhongtai Qi, Hao Su, Kaichun Mo, and Leonidas J. Guibas. 2017. PointNet: Deep Learning on Point Sets for 3D Classification and Segmentation. In *2017 IEEE Conference on Computer Vision and Pattern Recognition, CVPR 2017, Honolulu, HI, USA, July 21-26, 2017*. IEEE Computer Society, 77–85. <https://doi.org/10.1109/CVPR.2017.16>
- Urs Ramer. 1972. An iterative procedure for the polygonal approximation of plane curves. *Computer graphics and image processing* 1, 3 (1972), 244–256. [https://doi.org/10.1016/S0146-664X\(72\)80017-0](https://doi.org/10.1016/S0146-664X(72)80017-0)
- A Galvão Ramos, José F Oliveira, José F Gonçalves, and Manuel P Lopes. 2016. A container loading algorithm with static mechanical equilibrium stability constraints. *Transportation Research Part B: Methodological* 91 (2016), 565–581.
- Nicolas Ray, Jean-Christophe Ulysse, Xavier Cavin, and Bruno Levy. 2003. Generation of Radiosity Texture Atlas for Realistic Real-Time Rendering. In *Eurographics 2003 - Short Presentations*. Eurographics Association. <https://doi.org/10.2312/egs.20031064>
- Colin Rennie, Rahul Shome, Kostas E. Bekris, and Alberto F. De Souza. 2016. A Dataset for Improved RGBD-Based Object Detection and Pose Estimation for Warehouse Pick-and-Place. *IEEE Robotics and Automation Letters* 1, 2 (2016), 1179–1185. <https://doi.org/10.1109/LRA.2016.2532924>
- Daniel Saakes, Thomas Cambazard, Jun Mitani, and Takeo Igarashi. 2013. PacCAM: material capture and interactive 2D packing for efficient material usage on CNC cutting machines. In *The 26th Annual ACM Symposium on User Interface Software and Technology, UIST'13, St. Andrews, United Kingdom, October 8-11, 2013*, Shahram Izadi, Aaron J. Quigley, Ivan Poupyrev, and Takeo Igarashi (Eds.). ACM, 441–446. <https://doi.org/10.1145/2501988.2501990>
- Tom Schaul, John Quan, Ioannis Antonoglou, and David Silver. 2016. Prioritized Experience Replay. In *4th International Conference on Learning Representations, ICLR 2016, San Juan, Puerto Rico, May 2-4, 2016, Conference Track Proceedings*, Yoshua Bengio and Yann LeCun (Eds.). <http://arxiv.org/abs/1511.05952>
- Nico Schertler, Daniele Panozzo, Stefan Gumhold, and Marco Tarini. 2018. Generalized motorcycle graphs for imperfect quad-dominant meshes. *ACM Transactions on Graphics* 37, 4 (2018). <https://doi.org/10.1145/3197517.3201389>
- John Schulman, Filip Wolski, Prafulla Dhariwal, Alec Radford, and Oleg Klimov. 2017. Proximal Policy Optimization Algorithms. *CoRR* abs/1707.06347 (2017). <http://arxiv.org/abs/1707.06347>
- Steven S. Seiden. 2002. On the online bin packing problem. *Journal of the ACM (JACM)* 49, 5 (2002), 640–671. <https://doi.org/10.1145/585265.585269>
- Rahul Shome, Wei N. Tang, Changkyu Song, Chaitanya Mitash, Hristiyan Kourtev, Jingjin Yu, Abdeslam Boularias, and Kostas E. Bekris. 2019. Towards Robust Product Packing with a Minimalistic End-Effector. In *2019 International Conference on Robotics and Automation (ICRA)*. 9007–9013. <https://doi.org/10.1109/ICRA.2019.8793966>
- Arjun Singh, James Sha, Karthik S. Narayan, Tudor Achim, and Pieter Abbeel. 2014. BigBIRD: A large-scale 3D database of object instances. In *2014 IEEE International Conference on Robotics and Automation, ICRA 2014, Hong Kong, China, May 31 - June 7, 2014*. IEEE, 509–516. <https://doi.org/10.1109/ICRA.2014.6906903>
- David Stutz and Andreas Geiger. 2020. Learning 3D Shape Completion Under Weak Supervision. *International Journal of Computer Vision* 128, 5 (2020), 1162–1181. <https://doi.org/10.1007/s11263-018-1126-y>
- Satoshi Suzuki and Keiichi Abe. 1985. Topological structural analysis of digitized binary images by border following. *Computer vision, graphics, and image processing* 30, 1 (1985), 32–46. [https://doi.org/10.1016/0734-189X\(85\)90016-7](https://doi.org/10.1016/0734-189X(85)90016-7)
- Santosh Tiwari, Georges Fadel, and Peter Fenyes. 2010. A fast and efficient compact packing algorithm for SAE and ISO luggage packing problems. *Journal of Computing and Information Science in Engineering* 10, 2 (2010), 021010. <https://doi.org/10.1115/1.3330440>
- Petar Velickovic, Guillem Cucurull, Arantxa Casanova, Adriana Romero, Pietro Liò, and Yoshua Bengio. 2018. Graph Attention Networks. In *6th International Conference on Learning Representations, ICLR 2018, Vancouver, BC, Canada, April 30 - May 3, 2018, Conference Track Proceedings*. OpenReview.net. <https://openreview.net/forum?id=rjXmpikCZ>
- Fan Wang and Kris Hauser. 2019. Stable Bin Packing of Non-convex 3D Objects with a Robot Manipulator. In *International Conference on Robotics and Automation, ICRA 2019, Montreal, QC, Canada, May 20-24, 2019*. IEEE, 8698–8704. <https://doi.org/10.1109/ICRA.2019.8794049>
- Fan Wang and Kris Hauser. 2021. Robot Packing With Known Items and Nondeterministic Arrival Order. *IEEE Transactions on Automation Science and Engineering* 18, 4 (2021), 1901–1915. <https://doi.org/10.1109/TASE.2020.3024291>
- Fan Wang and Kris Hauser. 2022. Dense Robotic Packing of Irregular and Novel 3D Objects. *IEEE Trans. Robotics* 38, 2 (2022), 1160–1173. <https://doi.org/10.1109/TRO.2021.3097261>
- Ziyu Wang, Tom Schaul, Matteo Hessel, Hado van Hasselt, Marc Lanctot, and Nando de Freitas. 2016. Dueling Network Architectures for Deep Reinforcement Learning. In *Proceedings of the 33rd International Conference on Machine Learning, ICML 2016, New York City, NY, USA, June 19-24, 2016 (JMLR Workshop and Conference Proceedings, Vol. 48)*, Maria-Florina Balcan and Kilian Q. Weinberger (Eds.). JMLR.org, 1995–2003. <http://proceedings.mlr.press/v48/wangf16.html>
- Ziqi Wang, Peng Song, and Mark Pauly. 2021. MOCCA: modeling and optimizing cone-joints for complex assemblies. *ACM Transactions on Graphics (TOG)* 40, 4 (2021), 1–14. <https://doi.org/10.1145/3450626.3459680>



- Yuhuai Wu, Elman Mansimov, Roger B. Grosse, Shun Liao, and Jimmy Ba. 2017. Scalable trust-region method for deep reinforcement learning using Kronecker-factored approximation. In *Advances in Neural Information Processing Systems 30: Annual Conference on Neural Information Processing Systems 2017, December 4-9, 2017, Long Beach, CA, USA*, Isabelle Guyon, Ulrike von Luxburg, Samy Bengio, Hanna M. Wallach, Rob Fergus, S. V. N. Vishwanathan, and Roman Garnett (Eds.), 5279–5288. <https://proceedings.neurips.cc/paper/2017/hash/361440528766bbaaa1901845cf4152b-Abstract.html>
- Zifei Yang, Shuo Yang, Shuai Song, Wei Zhang, Ran Song, Jiyu Cheng, and Yibin Li. 2021. PackerBot: Variable-Sized Product Packing with Heuristic Deep Reinforcement Learning. In *IEEE/RSJ International Conference on Intelligent Robots and Systems, IROS 2021, Prague, Czech Republic, September 27 - Oct. 1, 2021*. IEEE, 5002–5008. <https://doi.org/10.1109/IROS51168.2021.9635914>
- Miaojun Yao, Zhili Chen, Linjie Luo, Rui Wang, and Huamin Wang. 2015. Level-set-based partitioning and packing optimization of a printable model. *ACM Transactions on Graphics (TOG)* 34, 6 (2015), 1–11. <https://doi.org/10.1145/2816795.2818064>
- Hang Yin, Anastasia Varava, and Danica Kragic. 2021. Modeling, learning, perception, and control methods for deformable object manipulation. *Science Robotics* 6, 54 (2021), 8803. <https://doi.org/10.1126/scirobotics.abd8803>
- Andy Zeng, Pete Florence, Jonathan Tompson, Stefan Welker, Jonathan Chien, Maria Attarian, Travis Armstrong, Ivan Krasin, Dan Duong, Vikas Sindhwani, and Johnny Lee. 2020. Transporter Networks: Rearranging the Visual World for Robotic Manipulation. In *4th Conference on Robot Learning, CoRL 2020, 16-18 November 2020, Virtual Event / Cambridge, MA, USA (Proceedings of Machine Learning Research, Vol. 155)*, Jens Kober, Fabio Ramos, and Claire J. Tomlin (Eds.). PMLR, 726–747. <https://proceedings.mlr.press/v155/zeng21a.html>
- Chi Zhang, Mao-Feng Xu, Shuangming Chai, and Xiao-Ming Fu. 2020. Robust atlas generation via angle-based segmentation. *Computer Aided Geometric Design* 79 (2020), 101854. <https://doi.org/10.1016/j.cagd.2020.101854>
- Hang Zhao, Qijin She, Chenyang Zhu, Yin Yang, and Kai Xu. 2021. Online 3D Bin Packing with Constrained Deep Reinforcement Learning. In *Thirty-Fifth AAAI Conference on Artificial Intelligence, AAAI 2021, EAAI 2021, Virtual Event, February 2-9, 2021*. AAAI Press, 741–749. <https://ojs.aaai.org/index.php/AAAI/article/view/16155>
- Hang Zhao, Yang Yu, and Kai Xu. 2022a. Learning Efficient Online 3D Bin Packing on Packing Configuration Trees. In *International Conference on Learning Representations*. <https://openreview.net/forum?id=bfuGjCwAq>
- Hang Zhao, Chenyang Zhu, Xin Xu, Hui Huang, and Kai Xu. 2022b. Learning practically feasible policies for online 3D bin packing. *Science China Information Sciences* 65, 1 (2022). <https://doi.org/10.1007/s11432-021-3348-6>



for some open neighborhood  $\mathcal{N}(p)$  of  $p$  and some direction  $d \in \mathbb{R}^2$ . The following property is an immediate consequence of the Minkowski sum, which establishes a direct connection between packing tightness and reference points in  $E$ :

PROPOSITION A.1. *If Equation 4 holds for some open neighborhood  $\mathcal{N}(p)$ , then:*

$$p = \operatorname{argmax}_{q \in \mathcal{N}(p)} d^T q \quad (5)$$

In other words, if  $d^T p$  is local optima, i.e.  $d^T p \geq d^T q$  for all  $q \in \mathcal{N}(p)$ , the point  $p$  corresponds to the most extreme placement of  $G$  in its neighborhood. With this tool at hand, we can directly evaluate and compare the potential packing tightness of a point  $p$  by looking at the range of directions  $d$  that makes  $p$  satisfy Equation 5.

Such a range of  $d$  corresponds exactly to the spanning angle of a 2D normal cone [Boyd et al. 2004]. The normal cone of a set  $C$  at a boundary point  $x_0$  is the set of all vectors  $y$  such that  $y^T(x - x_0) \leq 0$  for all  $x \in C$ . We summarize its property below:

PROPOSITION A.2. *For a convex polygonal set  $E$  and  $p \in \partial E$ , the spanning angle of the normal cone at  $p$  is defined as  $\tau(p) \triangleq \pi - \theta$ , where  $\theta$  is the interior angle of  $E$  at  $p$ .*

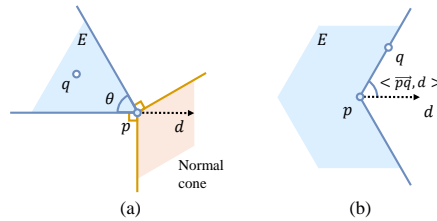


Fig. 17. (a): For a boundary point  $p$  on a convex cone  $E$ , arbitrary direction  $d$  in its normal cone satisfy  $d^T p \geq d^T q$ , where  $q \in E$ . (b): If  $p$  locates on a concave polygon part, for  $\forall d \in \mathbb{R}^2$ , there exists  $q \in E$  that  $\langle \vec{pq}, d \rangle$  is less than  $\pi/2$ , i.e.  $d^T p < d^T q$ .

A demonstration of a normal cone is provided in Fig. 17a. For a concave polygon, points located on its concave parts have no normal cone, and we extend that  $\tau(p) = 0$  in this case, as shown in Fig. 17b. Using  $\tau(p)$  as a tightness metric, we compare different choices of  $p$ . The following property is obvious:

THEOREM A.3. *For a polygonal set  $E$  and a convex  $p \in \partial E$ , we have  $p = \operatorname{argmax}_{q \in \mathcal{N}(p)} \tau(q)$  for some open neighborhood  $\mathcal{N}(p)$  of  $p$ .*

PROOF. Normal cones only exist on boundary points of the polygon and not the internal ones. Therefore, we could consider a neighborhood  $\mathcal{N}(p)$  containing  $p$  and  $p$ 's two neighboring edges, without any other convex vertices included. Within  $\mathcal{N}(p)$ ,  $p$  is convex so  $\tau(p) > 0$ . All other points  $q$  are on a straight line or concave vertices, with  $\tau(q) = 0$ .  $\square$

We demonstrate some neighborhoods in Fig. 18. Each convex vertex  $p$  corresponds to the local optima of  $\tau(p)$  and a tight object placement against obstacles. Based on the above observations, our candidate set consists of all convex vertices of  $E$ .

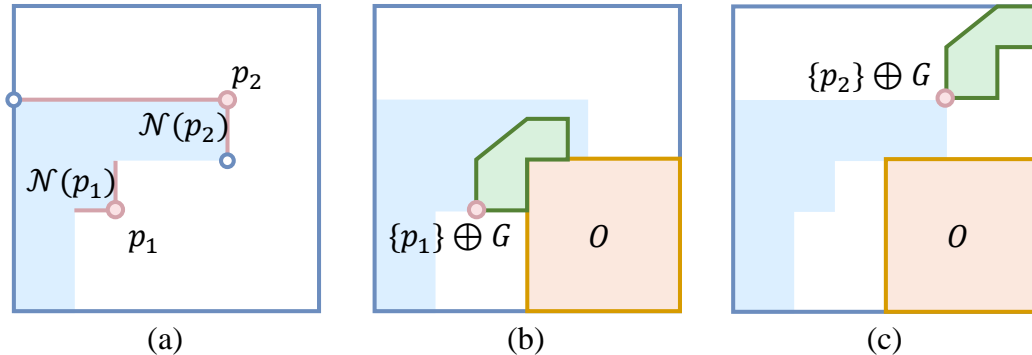


Fig. 18. (a): The pink parts are neighborhoods  $\mathcal{N}(p_1)$  and  $\mathcal{N}(p_2)$  for convex vertex  $p_1$  and  $p_2$ . Both  $\tau(p_1)$  and  $\tau(p_2)$  are local optima and they correspond to object placements, (b) and (c), tightly against obstacles.

## B PIPELINE FOR DATA PREPARATION

We aim at learning physically realizable packing (PRP) skills for general 3D shapes, which can be collected either by synthetic modeling or real-world scanning. For this, we first need to process task shapes into a compatible format for efficient and accurate simulation with the Bullet simulator [Coumans and Bai 2016]. We also need the planar-stable object poses to satisfy the robot manipulation stipulations. We outline our specific data preparation pipeline in Algorithm 2, where a polygonal mesh is transformed into several watertight convex decompositions and its planar-stable poses are provided. Considering that some stable poses are rotation-symmetric, we propose Algorithm 3 to remove redundant poses to avoid unbalanced shape distribution.

---

### ALGORITHM 2: Object Data Preparation

---

- 1: **Input:** A polygonal mesh  $M$  obtained by arbitrary approaches.
  - 2: **if**  $M$  is not watertight **then**
  - 3:   Reconstruct  $M$  [Stutz and Geiger 2020] to ensure watertightness.
  - 4: Compute all possible planar-stable poses  $\mathbf{P}$  [Goldberg et al. 1999] of  $M$ .
  - 5: Decompose  $M$  into several convex parts [Mamou et al. 2016] if non-convex. This step also simplifies  $M$  with fewer vertices, which benefits collision detections for simulation.
  - 6: Place the decomposed  $M$  in the simulator [Coumans and Bai 2016] with poses in  $\mathbf{P}$ . Remove poses which are factually unstable.
  - 7: Remove redundant rotation-symmetric poses in  $\mathbf{P}$  with Algorithm 3.
  - 8: **Return** Convex decompositions of  $M$  and  $\mathbf{P}$ .
- 

## C MORE EXPERIMENTAL RESULTS

### C.1 Effects of Experimental Parameters

Our packing experiment setup involves a set of parameters for finding candidates and describing packing observations. Here we refine these parameters to make ablation and study their effect on the final packing performance. We conduct this experiment on our main dataset *General*. We double the number of points sampled from object surfaces to 2048 and the candidate number  $N$  to 1000. For the intervals  $\Delta_h$ ,  $\Delta_\theta$ ,  $\Delta_z$ , and  $\Delta_g$  used to find candidates, we halve them to investigate whether finer action can lead to better performance.

**ALGORITHM 3:** Remove Redundant Planar-Stable Poses

---

```

1: Input: A watertight mesh  $M$ , poses  $\mathbf{P}$ , and a percentage constant  $c$ .
2: Valid pose set  $\mathbf{P}_v \leftarrow \emptyset$ , occupancy label set  $\mathbf{L} \leftarrow \emptyset$ .
3: for each pose  $p \in \mathbf{P}$  do
4:   Place  $M$  with  $p$  and rotate  $M$  vertically with the condition  $s_x \leq s_y$  and  $m_x \leq m_y$  until the smallest AABB volume is reached.
   Here  $s$  is the AABB size of  $M$  and  $m$  the mass center. Rewrite  $p \in \mathbf{P}$ .
5: Calculate the maximal AABB size after rotation. Denoted the size maximum along each dimension  $d_x, d_y$ , and  $d_z$ .
6: Voxelize the space in the range  $[0, d_x] \times [0, d_y] \times [0, d_z]$ .
7: for each rotated pose  $p \in \mathbf{P}$  do
8:   Move  $M$  with the FLB corner of its AABB aligned to the origin.
9:   Check if each space voxel is occupied by  $M$  with pose  $p$ . Denote the occupancy of all voxels as  $l_p$ .
10:  if no  $l \in \mathbf{L}$  make  $\sum f_x(l, l_p) / \sum l_p \leq c$ , where  $f_x$  is the xor function then
11:    Insert  $p$  into  $\mathbf{P}_v$  and insert  $l_p$  into  $\mathbf{L}$ .
12: Return  $\mathbf{P}_v$ .

```

---

Table 6. This table studies the effects of finer experimental parameters.

Parameters	Uti.	Var.	Num.	Time
Baseline	44.5%	3.4	27.7	0.04
Double Point Cloud Number	42.2%	2.1	26.3	0.04
Double Candidate Actions $N$	42.6%	2.0	26.5	0.04
Half Heightmap Interval $\Delta_h$	43.8%	2.3	27.0	0.13
Half Rotation Interval $\Delta_\theta$	42.1%	2.1	26.3	0.07
Half Height Interval $\Delta_z$	42.2%	2.3	26.3	0.05
Half Pixel Interval $\Delta_g$	44.8%	2.3	27.8	0.13

We summarize the test results in Table 6. Halving the pixel interval  $\Delta_g$  used to sample grid points has improvement to the packing performance, but it also substantially increases the time for decision-making. Finer tuning of other parameters no longer has a clear impact and may increase the computational overheads. We choose a set of efficient and effective parameters to do our main experiments.

## C.2 Ablations on RL Training

Here we do ablation studies to demonstrate the efficacy of our asynchronous RL training. We provide policies trained with the vanilla Rainbow as a baseline. We remove the distributed learner and the non-blocking actor equipped with batched simulation to illustrate their effect. We also report the performance without transforming the point cloud observation to a canonical configuration. All these policies are trained within 48 hours for fairness. From the test results summarized in Table 7, we can see that our asynchronous training achieves the best performance. Removing the canonical transform affects the data efficiency and lowers the packing utility.

## C.3 Results on Shapes from ABC

We test our method on shapes collected from the ABC dataset [Koch et al. 2019]. These shapes are mostly complex mechanical parts with distinct characteristics, as shown in Fig. 19. Totally 136 industrial shapes with 440 planar-stable poses are collected. We train an online packing policy and compare it with the existing heuristic competitors to

Table 7. Advantages of our asynchronous reinforcement learning training fashion. This experiment is conducted on the *General* dataset.

Training Variant	Uti.	Gap	Var.	Num.
The Vanilla Rainbow	41.3%	7.2%	<b>2.3</b>	25.7
No Distributed Learner	42.9%	3.6%	3.3	26.8
No Batched Simulation	41.3%	7.2%	3.3	26.0
No Canonical Transform	40.2%	9.7%	3.0	25.3
Our Asynchronous Training	<b>44.5%</b>	<b>0.0%</b>	3.4	<b>27.7</b>

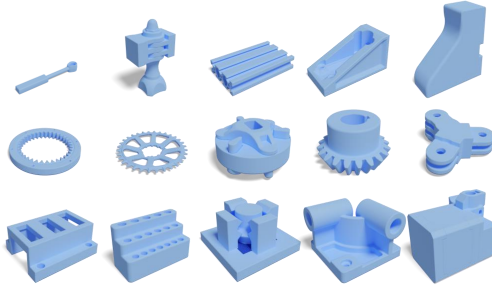


Fig. 19. Mechanical shapes selected from the ABC dataset. These shapes are scaled with their maximal AABB size equal to 1 for clarity.

Table 8. Packing performance on the shapes for the ABC dataset.

Method	Uti.	Gap	Var.	Num.	Time
Random	22.0%	35.3%	2.7	14.2	0.02
Random $\pi$	23.6%	30.6%	2.3	15.2	0.03
FF [1996]	25.0%	26.5%	2.5	16.0	0.03
MTPE [2015]	29.3%	13.8%	1.9	18.7	<b>0.03</b>
HM [2019]	27.4%	19.4%	2.0	17.5	0.03
BLBF [2020]	28.7%	15.6%	1.9	18.3	0.03
Ours	<b>34.0%</b>	<b>0.0%</b>	<b>1.9</b>	<b>22.6</b>	0.04
Ours (K = 3)	35.3%	-	1.7	23.5	0.06
Ours (K = 5)	37.4%	-	1.6	24.5	0.06
Ours (K = 10)	41.0%	-	1.7	25.5	0.06

demonstrate the superiority of our method. We also train the object-ordering and the placement policy pairs for solving buffered packing problems. We train these policy pairs with buffer size  $K = 10$  and generalize them to buffered packing scenarios with  $K = 3$  and  $K = 5$ . We report these results in Table 8.

#### C.4 Generalization between Datasets

We test generalization between datasets, that is, crossly test trained policies on other datasets. Since part of the shapes is shared between *General* and *Kitchen*, we conduct this experiment among *General*, shapes from the ABC dataset, and

Table 9. Generalize the trained policies to new datasets. The random performance and the best heuristic performance are also listed here.

Train	<i>General</i>			<i>ABC</i>			<i>BlockOut</i>		
	Uti.	Var.	Num.	Uti.	Var.	Num.	Uti.	Var.	Num.
<i>General</i>	44.5%	3.4	27.7	33.7%	1.7	22.4	67.5%	1.6	33.2
<i>ABC</i>	43.3%	4.1	27.2	34.0%	1.9	22.6	66.1%	1.4	32.4
<i>BlockOut</i>	38.0%	3.7	24.2	29.7%	1.4	20.0	71.0%	1.7	34.8
<i>Random</i>	31.6%	5.8	19.6	22.0%	2.7	14.2	37.1%	3.4	17.8
<i>Heuristic</i>	37.3%	4.6	22.7	29.3%	1.9	18.7	61.9%	4.1	29.5

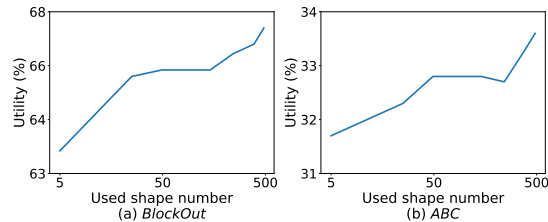


Fig. 20. Training policies with more shapes from *General* benefits the performance when being generalized to the other two datasets. *BlockOut*, with 483, 136, and 8 shapes respectively. These results are summarized in Table 9. When being transferred to a new dataset, the trained policies can still show decision-making ability more competitive than heuristics.

We note that policies trained on datasets with more variety of shapes tend to perform better on one out-of-distribution dataset. To confirm this, we train policies with different numbers of shapes from *General* and test them on *ABC* and *BlockOut*. Results are visualized in Fig. 20. We can see that rich training shapes help policies transfer to the other two datasets. We recommend that users increase shape variety to enable better performance on out-of-distribution shapes.

#### D MORE VISUALIZED RESULTS

We provide more visualization results tested on all datasets mentioned above, i.e. the *General* dataset, the *BlockOut* dataset, the *Kitchen* dataset, as well as industrial shapes that come from the *ABC* dataset. We show galleries of online PRP results on each dataset in Fig. 21. We provide qualitative results of buffered packing policies with  $K = 10$  in Fig. 22. The generalized results on buffered packing scenarios with  $K = 3$  and  $K = 5$  are visualized in Fig. 23 and Fig. 24.

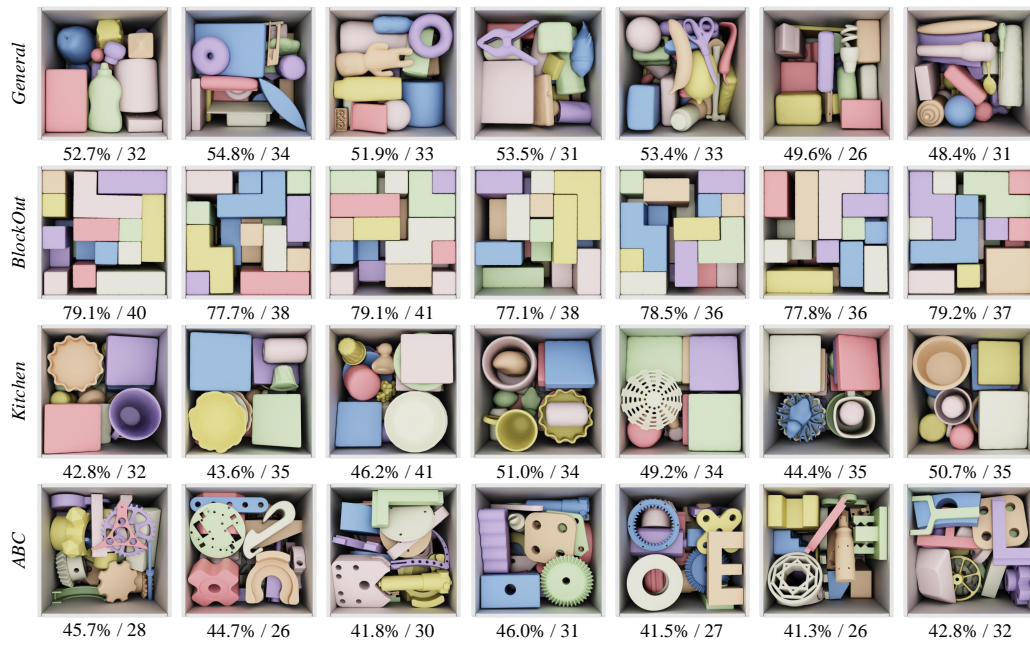


Fig. 21. Results generated by our online packing policies. Their utility and number of packed objects are labeled.

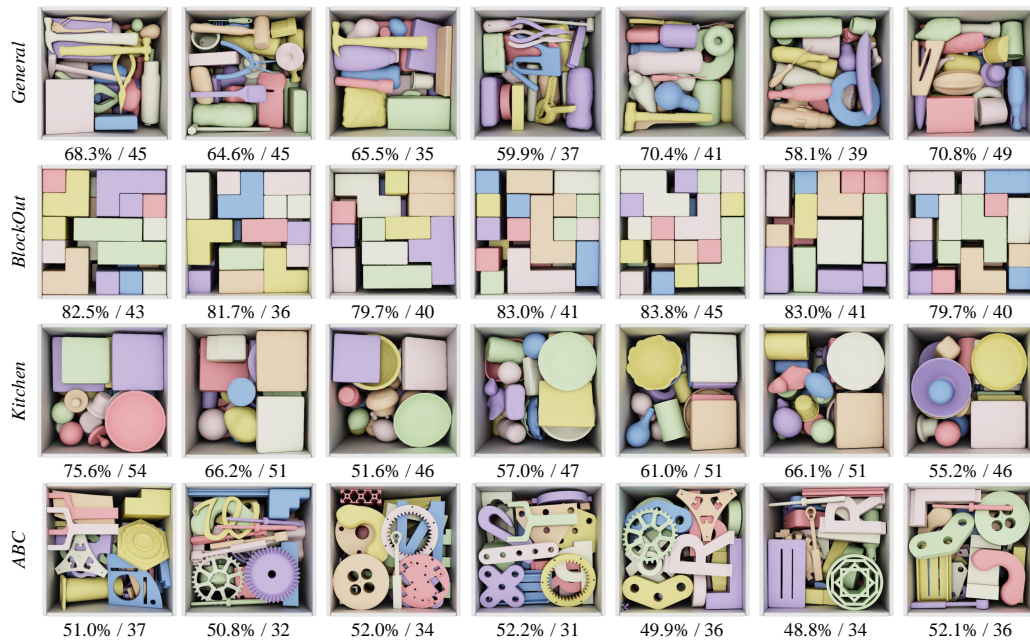


Fig. 22. Results generated by our buffered packing policies. These policies are trained and tested with a buffer size  $K = 10$ .



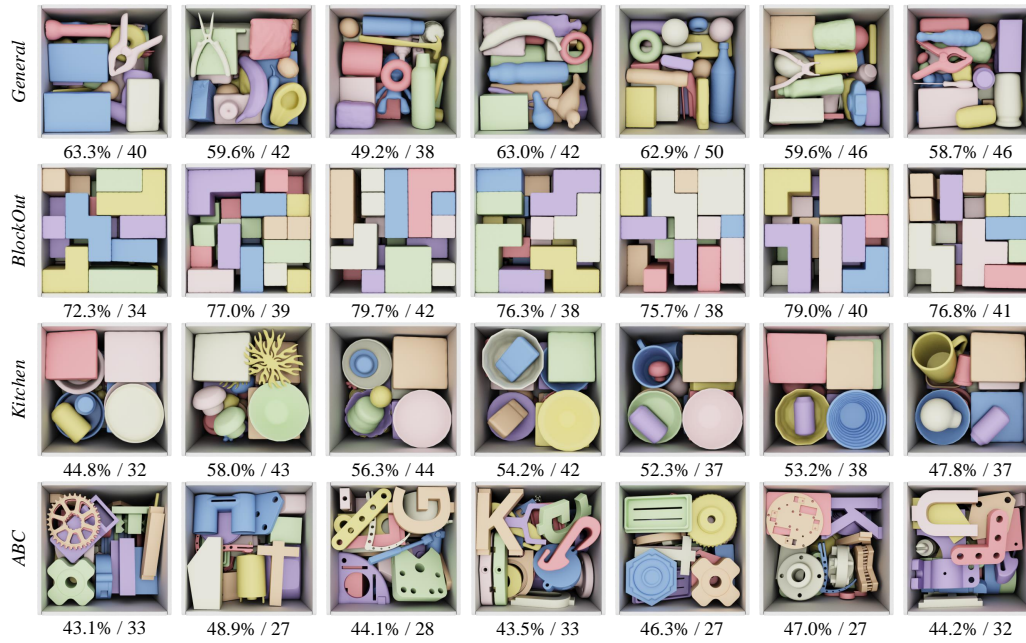


Fig. 23. Results generated by our buffered packing policies. These policies are trained with a buffer size  $K = 10$  and tested with  $K = 3$ .

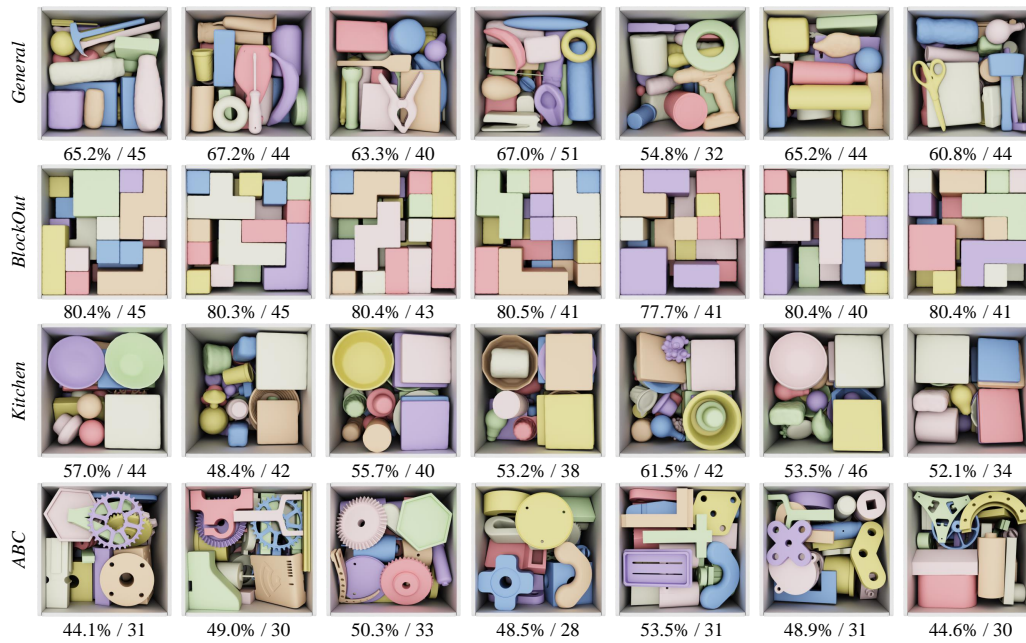


Fig. 24. Results generated by our buffered packing policies. These policies are trained with a buffer size  $K = 10$  and tested with  $K = 5$ .